Impact of Meteorology and Aerosol Sources on PM$_{2.5}$ and Oxidative Potential Variability and Levels in China

Jiemei Liu[1,2], Jesper H. Christensen[2], Zhuyun Ye[2], Shikui Dong[1], Camilla Geels[2], Jørgen Brandt[2], Athanasios Nenes[3,4], Yuan Yuan[1, *], and Ulas Im[2, *]

[1] Key Laboratory of Aerospace Thermophysics, Ministry of Industry and Information Technology, Harbin Institute of Technology, 92 West Dazhi Street, Harbin 150001, China

[2] Aarhus University, Department of Environmental Science/Interdisciplinary Centre for Climate Change, Frederiksborgvej 399, Roskilde, Denmark

[3] Laboratory of Atmospheric Processes and Their Impacts, Ecole Polytechnique Fédérale de Lausanne (EPFL), Lausanne, Switzerland

[4] Center for the Study of Air Quality and Climate Change, Foundation for Research and Technology Hellas (FORTH), Thessaloniki, Greece,

Correspondence: Yuan Yuan (yuanyuan83@hit.edu.cn) and Ulas Im (ulas@envs.au.dk)

Abstract: China has long-term high $PM_{2.5}$ levels, and its Oxidative Potential (OP) is worth studying as it may unravel the impacts of aerosol pollution on public health better than $PM_{2.5}$ alone. OP refers to the ability of $PM_{2.5}$ to induce oxidative stress (OS). OP and $PM_{2.5}$ are influenced by meteorological factors, anthropogenic emissions sources and atmospheric aging. Although their impact on $PM_{2.5}$ have been studied, OP measurements only recently became available and on a limited scale, as they require considerable technical expertise and resources. For this, the joint relationship between $PM_{2.5}$ and OP for a wide range of meteorological conditions and emissions profiles remain elusive. Towards this, we estimated $PM_{2.5}$ and OP over China using the Danish Eulerian Hemispheric Model (DEHM) system with meteorological input from WRF weather forecast model. It was found that higher values of $PM_{2.5}$ and OP were primarily concentrated in urban agglomerations in the central and eastern regions of China, while lower values were found in the western and northeastern regions. Furthermore, the probability density function revealed that about 40% of areas in China had an annual average $PM_{2.5}$ concentrations exceeding the Chinese concentrations limit. For OP, 36% of the regions have OP below 1 $nmol\ min^{-1}\ m^{-3}$, 41% have OP between 1 and 2 $nmol\ min^{-1}\ m^{-3}$, and 23% have OP above 2 $nmol\ min^{-1}\ m^{-3}$, which are in line with previous measurement studies. Analysis of the simulations indicate that meteorological conditions contributed 46% and 65% to $PM_{2.5}$ concentrations and OP variability, respectively, while anthropogenic emissions contributed 54% and 35% to $PM_{2.5}$ concentrations and OP variability, respectively. The emission sensitivity analysis also highlighted $PM_{2.5}$ and OP levels are mostly determined by secondary aerosol formation and biomass burning.

Keywords: $PM_{2.5}$; Oxidative potential; Meteorology; Anthropogenic emission sources; Probability density function

1. Introduction

Fine particulate matter, with an aerodynamic diameter of less than 2.5 μm ($PM_{2.5}$), is the primary

40 atmospheric pollutant in China (Chen et al., 2021; Chen et al., 2021; Liu et al., 2023) with respect to

human health. $PM_{2.5}$ exposure in China for 2017 resulted in an estimated 1.8 (95% CI: 1.6, 2.0) million

premature deaths (Liu et al., 2021). Many recent studies have suggested that the oxidative potential (OP)

of $PM_{2.5}$ may better explain the negative impact of $PM_{2.5}$ exposure on human health than the well-

established metric of mass concentrations (Yu et al., 2019; Gao et al., 2020). OP refers to the ability of

45 $PM_{2.5}$ to induce oxidative stress (OS) (Yang et al., 2021). Liu et al. (2020) summarized OP

measurements conducted in nine regions of China around 2014. The results showed that the average OP

content in northern Beijing was highest during the winter of 2016 (~14.0 $nmol\ min^{-1}\ m^{-3}$), while the

average OP level in Shanghai during the spring of 2016 was lowest (~0.15 $nmol\ min^{-1}\ m^{-3}$). However,

there is currently no exact threshold division of OP values. Exposure to high levels of OP (from

50 compounds such as quinones and soluble transitional metals) induces an excess production of reactive

oxygen species (ROS) in cells and lead to OS effects and ultimately trigger inflammation and disease.

Therefore, reducing $PM_{2.5}$ pollution and its associated OP (the volume-normalized dithiothreitol activity)

are critical to addressing China's environmental and environmental health issues.

Anthropogenic emissions, as the main source of $PM_{2.5}$ pollution and environmental health risks, have

55 been studied extensively (Chen et al., 2019; Liu et al., 2022). Zhu et al. (2018) and Pui et al. (2014)

summarized the studies on the PM sources in China and reported that secondary inorganic aerosols (SIA),

industry, residential combustion, biomass burning, industry, and transportation are the main source

categories in China in the historical and future business-as-usual scenarios. Due to the significant

influence of various sectors on $PM_{2.5}$ emissions, and research (Liu et al., 2018; Liu et al., 2020)

60 indicating a close association between $PM_{2.5}$ and OP, the connection between OP, serving as a toxicity

indicator for $PM_{2.5}$, and its sources (Liu et al., 2020) is becoming increasingly crucial and the topic of

numerous studies. For instance, Yu et al. (2019) used the dithiothreitol (DTT) assay to measure the $PM_{2.5}$

samples in Beijing throughout the year and identified vehicle emissions as the main contributing source

based on the source analysis of OP. However, studies conducted in three coastal cities of the Bohai Sea

65 region (Liu et al., 2018) and in Nanjing (Zhang et al., 2023) using the same DTT assay indicated that

coal combustion was the most active source of OP. Together, these studies suggest that obtaining the

spatial distribution characteristics of $PM_{2.5}$ and OP and their links to emission sources, is of paramount importance for implementing region-specific control measures.

Apart from anthropogenic emissions, meteorological conditions (i.e., temperature, humidity, wind speed, precipitation) also play a crucial role in the formation, accumulation, transformation, and dispersion of $PM_{2.5}$ (Liu et al., 2022; Liu et al., 2022). Utilizing a multiple linear regression model, Gong et al. (2022) conducted an analysis of the trends of meteorological elements and $PM_{2.5}$ levels across various regions in China from 2013 to 2020. Furthermore, they separated and quantified the impacts of meteorological factors and emissions on these trends. The findings indicate that meteorology alone can account for approximately 20~33% of the variability in $PM_{2.5}$ levels. Xing et al. (2023) conducted a study in the Shenzhen region using DTT, ascorbic acid (AA), and glutathione (GSH) OP assays. They analyzed meteorological conditions and $PM_{2.5}$ chemical composition to understand how the prevalence of monsoons in winter (northern and northeastern winds) and summer (southern and southeastern winds) affected the sources and contributed to the seasonal variation in $PM_{2.5}$ composition and OP (mass-normalized). Similarly, Molina et al. (2023) and Wang et al. (2019) revealed that meteorological conditions indirectly influence OP (volume-normalized and mass-normalized) through their impact on the chemical properties of the components. Ainur et al. (2023) employing a DTT assay, investigated outdoor health risks associated with atmospheric particulate matter in Xi'an, find a positive correlation between winter OP (volume-normalized) and relative humidity. Although several studies have identified linkages between meteorological conditions and $PM_{2.5}$/OP, quantitative assessment of meteorological conditions to both $PM_{2.5}$ and OP variability is lacking.

As of the present, research on the influence of both meteorological conditions and anthropogenic emissions on OP primarily relies on measurement methods (Yu et al., 2019; Gao et al., 2020; Campbell et al., 2021), such as DTT, AA, and GSH, which are difficult and costly to test and hard to provide the spatial distribution of OP comprehensively. Although mechanistic models of OP do exist (Shahpoury et al., 2024), their links to experimental metrics of OP are qualitative. For this, we propose a hybrid approach combining existing observations of OP with a chemistry transport model (CTM). So, using OP from assays and their observed links to sources and chemical constituents can then be parameterized and implemented in CTM for a comprehensive assessment of OP exposure over large areas and time periods.

This study quantifies the contribution of meteorological and anthropogenic emission factors (i.e., coal combustion, biomass burning, secondary aerosol formation that originate from a series of atmospheric

reactions, industry, and transportation source) to OP and $PM_{2.5}$ levels throughout China with the Danish

Eulerian Hemispheric Model (DEHM) model. The study hence provides a method for calculating OP

across China and using OP as an indicator to assess the impacts of anthropogenic emission sources on

100   human health in China.

2. Materials and methods

2.1 Methodological flow

The research strategy of this study consists of three main parts: model setup, spatial distribution

characteristic analysis, and quantification of meteorological conditions and anthropogenic emissions'

105   contributions (Figure 1). In the first part, DEHM was employed to obtain hourly pollutant concentrations,

followed by model evaluation, where the numerical weather prediction model WRF v4.1 (Skamarock et

al., 2008) driven by either ERA5 or global climate data from CESM was used as meteorological input

to DEHM and with exactly same spatial setup for China as in DEHM. Sensitivity experiments were

designed for meteorological conditions, emission inventories, and anthropogenic emission sources. From

110   these simulations, the spatial-scale estimation of OP was estimated by incorporating simulated values of

primary and secondary $PM_{2.5}$ concentrations from various anthropogenic sources into Equation (1) (see

Sect.2.2 for detail).
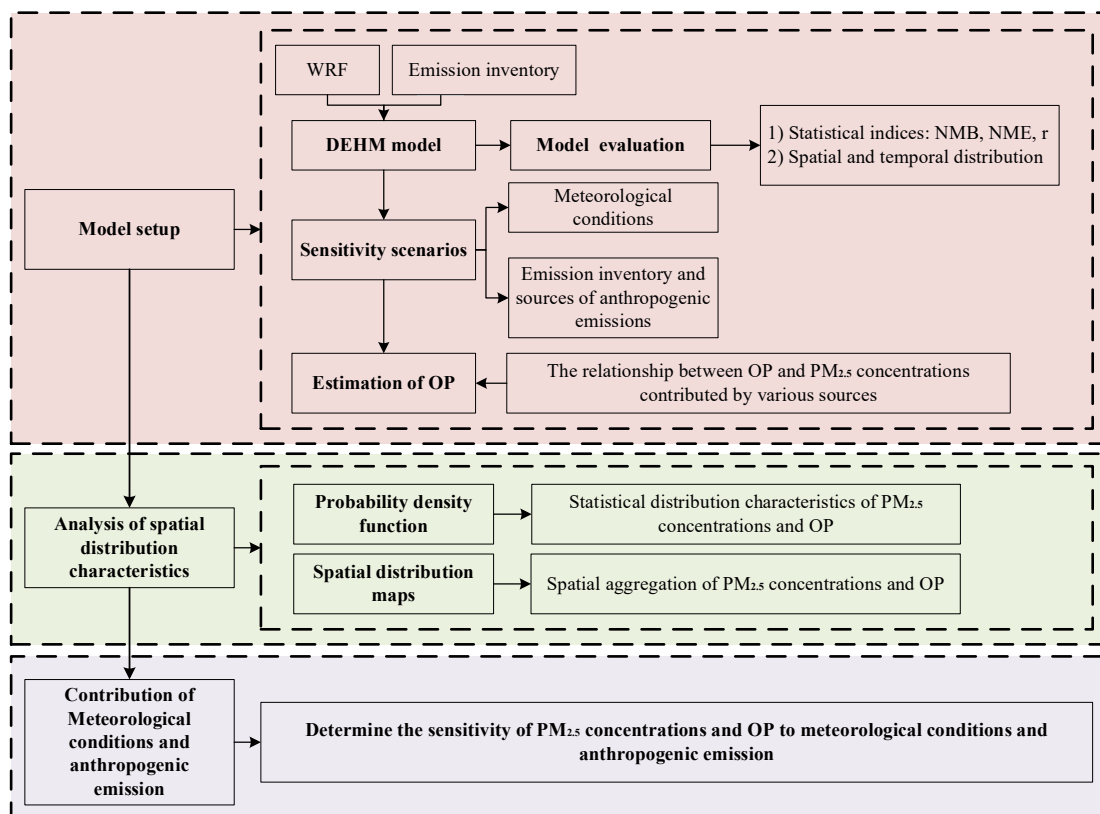
Figure 1. Schematic diagram of the study strategy; NME, NMB, r, and OP are normalized mean error, normalized mean bias, correlation coefficient, and oxidative potential, respectively.

In the second part, the spatial distribution characteristics of $PM_{2.5}$ and OP were determined using probability density functions (PDF) and spatial distribution maps. In the third part, quantitative analysis was conducted based on the simulation results from the sensitivity experiments to determine the extent of influence of meteorology and emissions on $PM_{2.5}$ and OP, as well as the primary sources of $PM_{2.5}$ and OP.

2.2 Estimation of OP

Most of current data on OP of $PM_{2.5}$ in China are obtained by means of measurement, and the research objects are basically limited to specific cities, which to some extent hinders the conduct of research on OP in a large-scale region. Considering that Liu et al. (2018) collected samples across four seasons from multiple representative locations in China, their developed OP prediction model (Equation (1)) can support us in estimating OP (with a unit of $nmol\ min^{-1}\ m^{-3}$) in China, thereby exploring the spatial distribution characteristics of OP and the contributions of different anthropogenic sources to OP. In the present study, we have used this relationship, in combination with the sensitivity simulations (Sect. 2.4), to calculate the OP.

$$OP = 0.088 \times re + 0.076 \times bi + 0.041 \times se + 0.034 \times in + 0.017 \times tr \qquad (1)$$

where, re, bi, in, and tr represent the primary $PM_{2.5}$ concentrations (with a unit of $\mu g\ m^{-3}$) for coal combustion, biomass burning, industry source, and transportation source, respectively. se (secondary aerosol formation) refers to the concentrations of secondary organic and inorganic (SOA and SIA, respectively) components (with a unit of $\mu g\ m^{-3}$). In this study, the coal combustion refers to coal heating from the residential sector. Biomass burning includes open burning of agricultural biomass, domestic biomass burning for cooking and heating, and biomass burning from biomass power plants and coal-fired power plants. Industry source is mainly derived from specific industrial processes in the iron and steel industrial base, metallurgical production plants for non-ferrous metals (e.g., titanium and molybdenum), and so on. Transportation source primarily comes from tailpipe emissions. It's worth mentioning that secondary aerosol formation originates from a series of atmospheric reactions. Some identified sources (i.e., coal combustion, biomass burning, industrial processes, and transportation) may generate secondary inorganic and organic aerosols through the emission of their precursor components. The coefficient (with a unit of $nmol\ min^{-1}\ m^{-3}\ source^{-1}$) reflect the intrinsic OP of each source.

2.3 Model setup

The DEHM can well capture many features of PM and its precursors' changes in large-scale space (Christensen, 1997; Brandt et al., 2012; Im et al., 2019). To date, the DEHM model has been widely used in air pollution and health risk assessment research in Europe and Asia (Brandt et al., 2013a; b; Zare et al., 2014; Geels et al., 2015; Im et al., 2018; Im et al., 2019; Lehtomäki et al., 2020; Cramer et al., 2020; Liu et al., 2021; Geels et al., 2021; Thomas et al., 2022; Im et al., 2023), but this will be the first time that DEHM is applied to estimate OP. Thus, The DEHM model system was used to simulate the pollutant concentrations in 2014 by using a two-way nested domain in this study (Kumar et al., 2016). A mother domain with a resolution of 150 km × 150 km was employed on a polar stereographic projection, true at 60°N to cover the entire Northern Hemisphere. The nested domain covered the whole of China consisting of 150 × 150 grid cells with a resolution of 50 km × 50 km, which was used for the analysis. The mother domain provided initial and boundary conditions for the nested domain. Vertically, there were 29 unevenly distributed layers, with the highest level reaching 100 hPa, and the lowest layer was approximately 20 m in height. The meteorological fields were simulated using the WRF model (Skamarock et al., 2008) with the same domain and resolution driven by global meteorological data

obtained from the ERA5 dataset and the Community Earth System Model (CESM) global model, respectively. The simulations utilized the Revised MM5 surface layer scheme, the Yonsei University

160   (YSU) boundary layer parameterization scheme (Hong et al., 2006), the Multi-scale Kain-Fritsch cumulus parameterization scheme (Zheng et al., 2016), the CAM longwave radiation scheme, the CAM shortwave radiation scheme (Skamarock et al., 2021), etc. The gas-phase chemistry module included 66 species, 9 primary particles (including natural particles such as sea salt), and 138 chemical reactions and was based on the scheme by Strand et al. (1994) (Brandt et al., 2012). The gas-phase species

165   considered in this study included SO_2, NO_2, CH_4, C_2H_6, etc. $PM_{2.5}$ was formed by BC, OC, sea salt, ammonium (NH_4^+), nitrate (NO_3^-), sulfate (SO_4^{2-}), and secondary organic aerosols (SOA), among others (Frohn et al., 2022). Biogenic volatile organic compounds (BVOCs), such as isoprene, contributed to the formation of SOA (Zare et al., 2012). Further details on the configuration of the chemical scheme and the list of chemical reactions can refer to the literature (Zare et al., 2012; Brandt et al., 2012; Collin,

170   2020; Frohn et al., 2022). The SOA were calculated using the volatility basis set (see details in Im et al. (2019)). In addition to the anthropogenic emissions, DEHM also includes emissions from biogenic emissions, such as vegetation, sea salt, lightning, soil, etc. The current version of the DEHM model does not include wind-blown, resuspended dust emissions or road dust nor aerosol-radiation or radiation-cloud interactions. The time resolution of the DEHM model output is one hour.

175   In the current study, the DEHM model used anthropogenic emissions from the Emissions Database for Global Atmospheric Research – Hemispheric Transport of Air Pollution (EDGAR-HTAP) database and Eclipse V6. The biomass burning emissions are obtained from the Global Fire Assimilation System (GFAS) from ECMWF (Kaiser et al., 2012), which has a horizontal resolution of a 0.1° × 0.1° on a daily time basis. Natural emissions for DEHM are based on the Global Emissions InitiAtive (GEIA, Zare et

180   al., 2012; Frost et al., 2013) with monthly inventories for emissions of nitrogen oxides from soil and lightning, and annual inventories for emissions of ammonia from natural sources. The production of sea salt (Soares et al., 2016) and biogenic volatile organic compounds (Zare et al., 2014) are calculated online in the model as a function of meteorological parameters like wind speed and temperature (Frohn et al., 2022).

185   **2.4 Sensitivity scenarios**

2.4.1 Relative contributions from meteorological conditions and emissions

Table 1 summarizes the scenarios for assessing the relative contributions of meteorological conditions and emissions to $PM_{2.5}$ and OP variability in 2014. ERA5 (Hersbach et al., 2020; ERA, 2023) is a global reanalysis dataset that is based on the assimilation of historical observations and model data. Studies

190   (Thomas et al., 2021; Xu et al., 2022) have demonstrated that ERA5 performs well relative to MERRA, NCEP, and ERA-Interim, with higher temporal and spatial resolutions. Therefore, Scenarios C_1 and C_2 used ERA5 as input to WRF. Considering the robust representation of aerosol effective radiative forcing and good predictive capabilities for key surface variables in CESM (2023) (García-Martínez et al., 2020; Richter et al., 2022), Scenario C_3 utilized meteorological data based on CESM version 2.1.1

195   (Danabasoglu et al., 2020) climate model as input for WRF. Scenarios C_2 and C_3 employed the Eclipse V6 emissions inventory, while Scenario C_1 used the EDGAR-HTAP inventory.

The ECLIPSE project by the International Institute for Applied Systems Analysis (IIASA) aims to generate a global gridded anthropogenic emission inventory for various emission scenarios. The Greenhouse Gas - Air Pollution Interactions and Synergies (GAINS) model has been employed to

200   estimate emissions of air pollutants and GHGs (such as SO_2, NO_x, NH_3, NMVOC, BC, OC, OM, $PM_{2.5}$, PM_{10}, CO, CH_4) using source characteristics and emission factors at a resolution of $0.5° \times 0.5°$ latitude-longitude (Upadhyay et al., 2020; Eclipse, 2020). The following sector-layers are available: energy, industry, solvent use, transport, domestic combustion, agriculture, open burning of agricultural waste, waste treatment. a number of scenarios are provided for which the key economic assumptions and energy

205   use originate from IEA World Energy Outlook (IEA, 2011), the POLES model, or Energy Technology Perspectives (IEA, 2012) for the period 2010-2050, while statistical data for the period 1990-2010 came from IEA. For agriculture the FAO databases and long-term global projections were used (Alexandratos et al., 2012). It is noteworthy that this inventory considers China's 13th 5-year plan.   The EDGAR-HTAP (Joint et al., 2011; Crippa et al., 2023) emission inventory endeavors to employ official or

210   scientific inventories within a national or regional scale, with a spatial resolution of $0.1° \times 0.1°$. EDGAR-HTAP comprehensively accounts for all major emission sectors, including residential, transportation, industrial, energy, and agricultural sectors. EDGAR offers independent emission estimates for various pollutants, including CO, CH_4, SO_2, NO_x, NMVOC, NH_3, $PM_{2.5}$, PM_{10}, BC, and OC. These estimates

follow a standardized methodology provided by the Intergovernmental Panel on Climate Change (IPCC).

215   The data from EDGAR allows for comparisons with emission reports published by European Member

States or Parties under the United Nations Framework Convention on Climate Change (UNFCCC)

(Kumar et al., 2023).

Equations (2~5) were used to quantitatively evaluate the contributions of meteorological conditions and

emission inventories.

$$\text{Con(Met)} = \frac{C_2 - C_3}{C_3} \tag{2}$$

$$\text{Con(Emi)} = \frac{C_1 - C_2}{C_2} \tag{3}$$

$$\text{NCon(Met)} = \frac{\text{abs(Con(Met))}}{\text{abs(Con(Met))} + \text{abs(Con(Emi))}} \tag{4}$$

$$\text{NCon(Emi)} = \frac{\text{abs(Con(Emi))}}{\text{abs(Con(Met))} + \text{abs(Con(Emi))}} \tag{5}$$

220   where, C_1, C_2 and C_3 represent the PM$_{2.5}$ concentrations and OP from scenarios C_1, C_2 and C_3,

respectively. Con(Met) represents the impact of changing meteorological datasets on changes in PM$_{2.5}$

and OP. Con(Emi) represents the impact of changing emission inventory on changes in PM$_{2.5}$ and OP.

NCon(Met) and NCon(Emi) represent the normalized contributions of meteorology and emission. In the

equations, the abs function represents the absolute value of the quantity in parentheses.

225   **Table 1. Emission inventory and meteorological datasets in three simulation scenarios.**

Scenarios	Emission inventory	Meteorological datasets
C_1	EDGAR-HTAP	ERA5
C_2	Eclipse V6	ERA5
C_3	Eclipse V6	CESM

2.4.2 Relative contributions from individual emissions

As mentioned above, OP's main source contributions include five parts, i.e., coal combustion, biomass

burning, secondary aerosol formation, industrial sources, and transportation sources (Equation (1)), we

conducted perturbation experiments targeting these five sources to quantitatively assess their

230   contributions to PM$_{2.5}$ concentrations and OP(Figure 2). These experiments were carried out within the

three scenarios described in Section 2.4.1, and we performed a total of 15 runs. Under the non-

perturbation condition (referred to as the NPC case), all aforementioned emission sources were

considered. Under the perturbation condition (referred to as the PC case), reduction designs were

implemented for emissions from coal combustion, biomass burning, industrial sources, and transportation sources. The emissions of both primary aerosols and tracegases from each individual source are reduced by 30%. The choice of 30 % was motivated by the consideration that the perturbation would be large enough to produce a sizeable impact (i.e., more than numerical noise) even at long distances, while small enough to be in the near-linear atmospheric chemistry regime (Galmarini et al., 2017; Im et al., 2019). Notably, the transportation sector in the DEHM model only considers tailpipe emissions, excluding non-exhaust emissions from vehicles like road dust, brake dust, and tire wear. The contribution of tailpipe emissions in the transportation sector to OP is estimated by incorporating simulated values of primary $PM_{2.5}$ concentrations from tailpipe emissions into Equation (1). In this study, the transportation sector refers to road transport, excluding other transportation sources like ships and airplanes. Additionally, to estimate the $PM_{2.5}$ concentrations and OP from coal and biomass burning, it is necessary to obtain the percentage contributions of $PM_{2.5}$ emissions from coal combustion for residential heating, domestic biomass burning for cooking and heating to $PM_{2.5}$ emissions of the residential sector, respectively, as well as the percentage contributions of $PM_{2.5}$ emissions from biomass burning in power plants to the total $PM_{2.5}$ emissions from the power sector. The percentage contributions of each anthropogenic source can be estimated using Equations (6~8).

$$PC_{re_{-j}} = \frac{E_{re\_j}}{E_{re}} \tag{6}$$

$$E_{pp_{-bi}} = EF \times FQ \tag{7}$$

$$PC_{pp\_bi\_cf} = \frac{E_{pp_{-bi}} + E_{pp\_cf}}{E_{pp}} \tag{8}$$

where, $PC_{re_{-j}}$ denotes the percentage contribution of $PM_{2.5}$ emissions from the residential subsector j (including coal cooking, coal heating, biomass cooking, biomass heating, clean energy, and nonresidential) to the total $PM_{2.5}$ emissions from the residential sector. E_{re_j} represents the $PM_{2.5}$ emissions from the residential subsector j, while E_{re} represents the total $PM_{2.5}$ emissions from the residential sector. The values of E_{re_j} and E_{re} are obtained from the literature (Yun et al., 2020). After calculation, the values for $PC_{re_{\text{coal cooking}}}$, $PC_{re_{\text{coal heating}}}$, $PC_{re_{\text{biomass cooking}}}$, and $PC_{re_{\text{biomass heating}}}$ are determined to be 21%, 27%, 33%, and 19%, respectively. $E_{pp_{-bi}}$ refers to the $PM_{2.5}$ emissions from biomass power plants, EF refers to the $PM_{2.5}$ emission factor of biomass power plants, and FQ refers to the fuel quantity. $PC_{pp\_bi\_cf}$ refers to the percentage contribution of $PM_{2.5}$ emissions from biomass power plants and coal-fired power plants to the $PM_{2.5}$ emissions of the power plants. To accelerate carbon

reduction in coal-fired power generation, the Chinese government has issued a series of policies supporting and encouraging the coupling of coal and biomass for power generation (Mao, 2017). This undoubtedly adds complexity to distinguishing between PM$_{2.5}$ emissions from coal combustion and biomass fuel. Furthermore, in the energy strategy where biomass serves as a clean alternative to fossil fuels, the scale of biomass utilization and the biomass power generation industry in China continue to expand (Lin et al., 2021). Considering the aforementioned reasons, we include PM$_{2.5}$ emissions from coal-fired power plants in our analysis. E_{pp_cf} refers to the PM$_{2.5}$ emissions from coal-fired power plants, and E_{pp} refers to the PM$_{2.5}$ emissions from power plants. EF, FQ, E_{pp_cf}, and E_{pp} are obtained from the literature (Zheng et al., 2018; Tong et al., 2018; Yun et al., 2020; MEE, 2020; Wang et al., 2020; Tang et al., 2020; Lin et al., 2021; Chen et al., 2022). After calculation, $PC_{pp\_bi\_cf}$ is determined to be 54%. Previous studies (Hodan et al., 2004; Chen et al., 2018; Zhang et al., 2022) showed that in China, the proportion of secondary and primary PM$_{2.5}$ mass to the total PM$_{2.5}$ mass is close, so we assume that they account for 50% respectively. Figure 2 showed the emission reduction design for perturbed emissions.
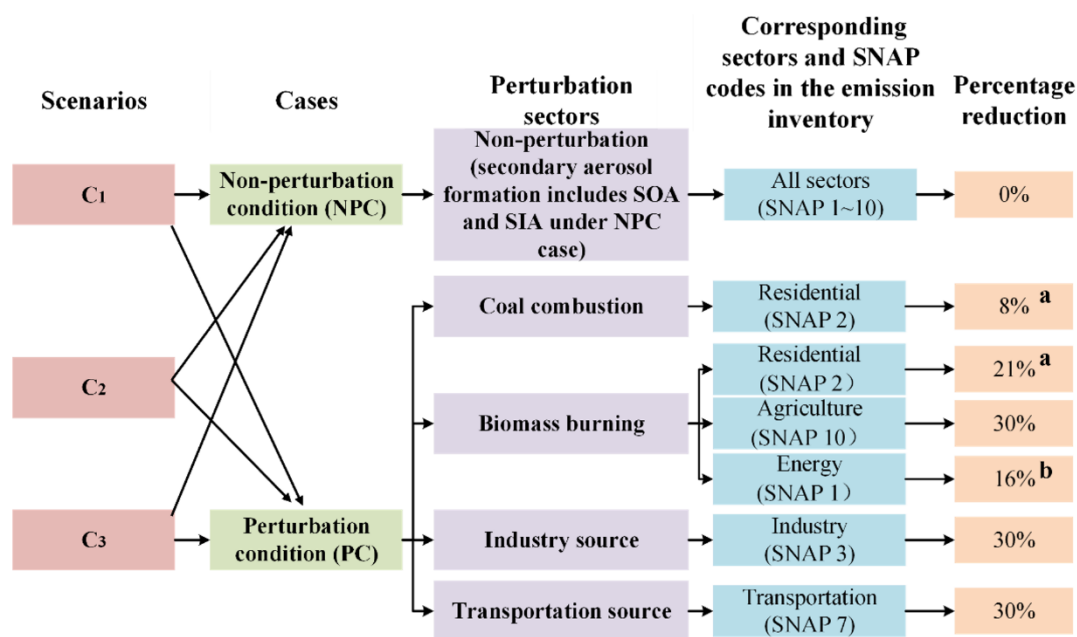
Figure 2. Emission reduction design for perturbed emissions; [a] was obtained from the literature (Yun et al., 2020), [b] were obtained from the literature (Zheng et al., 2018; Tong et al., 2018; Yun et al., 2020; MEE, 2020; Wang et al., 2020; Tang et al., 2020; Lin et al., 2021; Chen et al., 2022).

Furthermore, the PM$_{2.5}$ concentrations for each sector is calculated using Equations (9~11).

$$C_{P,i} = \frac{C_{NPC,i} - C_{PC,i}}{30\%} \tag{9}$$

$$C_{P,primary\ PM2.5} = C_{P,total\ PM2.5} - C_{P,SIA} - C_{P,SOA} \tag{10}$$

$$C_{secondary} = C_{NPC,SOA} + C_{NPC,SIA} \tag{11}$$

where, i refers to the type of pollutants, i.e., total PM$_{2.5}$, SOA, SIA, and primary PM$_{2.5}$. $C_{NPC,i}$ represents

280   concentrations of the pollutant i in the NPC case. $C_{PC,i}$ represents concentrations of the pollutant i in the

PC case. $C_{P,i}$ represents concentrations of the pollutant i by the specific emission sector P which is

perturbed (perturbation sectors P include coal combustion, biomass burning, industry, traffic source).

$C_{P,primary\ PM2.5}$ represents concentrations of primary PM$_{2.5}$ by the perturbation sectors P. $C_{secondary}$

represents PM$_{2.5}$ concentrations by the secondary aerosol formation.

285   **2.5 Probability density function**

Taking into account the substantial spatial heterogeneity of PM$_{2.5}$ concentrations and OP, we employ

PDF to characterize the statistical distribution characteristics of PM$_{2.5}$ concentrations and OP across

China. This offers a more generalized and robust probability for criteria limits. In this study, all three

functional types (Lognormal, exponential, and Gamma) were tested for annual average of PM$_{2.5}$

290   concentrations and OP at the monitoring stations. To determine the representative distributions for the

datasets, we further performed goodness-of-fit tests such as the Sum of Squared Error (SSE) and the

Kolmogorov-Smirnov (K-S) test (de Melo et al., 2000), using the fitter package in Python.

3. Results and discussion

3.1 Model evaluation

295   The hourly observation data was obtained from the Ministry of Ecology and Environment of China (MEE,

2014). The MEE website first released PM$_{2.5}$ measurement data in January 2013. In accordance with the

Chinese environmental protection standards, the hourly PM$_{2.5}$ concentrations are measured using the

micro-oscillation balance method and beta absorption method, with an uncertainty of less than

$5\ \mu g\ m^{-3}$ (Zeng et al., 2021). The PM$_{2.5}$ monitoring stations are primarily distributed in urban areas,

300   particularly in major metropolitan areas of China (Zeng et al., 2021). In 2014, the observation stations

are mainly concentrated in eastern China, while stations in western China are limited. Therefore, in the

present study, we also evaluated with the gridded annual-mean global reanalysis Dalhousie surface PM$_{2.5}$ dataset (van Donkelaar et al., 2021), which combines satellite retrievals of aerosol optical depth, chemical transport modeling, and ground-based measurements. The Dalhousie dataset compensated for

305   the non-uniform distribution spatially of observation stations to comprehensively evaluate the performance of the DEHM model. The density scatter plot of model performance and evaluation for China in scenario C$_1$ based on annual mean PM$_{2.5}$ observations from MEE and PM$_{2.5}$ derived from the Dalhousie dataset are shown in Figure 3. Overall, the model performance in terms of correlation coefficient (R) and normalized mean error (NME) calculated based on annual mean observations met the

310   performance criteria suggested by Emery et al. (2017) (NME<0.5, R>0.4), and the normalized mean bias (NMB) was also close to the performance criteria suggested by Emery et al. (2017) (NMB<±0.3). Compared to the observations, the model performance in terms of R, NME, and NMB calculated based on the Dalhousie dataset was slightly poorer but still close to the performance criteria suggested by Emery et al. (2017). Additionally, this study evaluated the model performance in scenarios C$_2$ and C$_3$

315   (Figure S2). It was found that under scenarios C$_2$ and C$_3$, the model performance in terms of R and NME, calculated based on both annual mean observations and Dalhousie dataset met the performance criteria suggested by Emery et al. (2017). The NMB under scenarios C$_2$ and C$_3$ calculated based on both annual mean observations and Dalhousie dataset were also close to the performance criteria suggested by Emery et al. (2017). Therefore, the simulated annual mean PM$_{2.5}$ concentrations in scenarios C$_1$, C$_2$ and C$_3$ are

320   considered reliable.
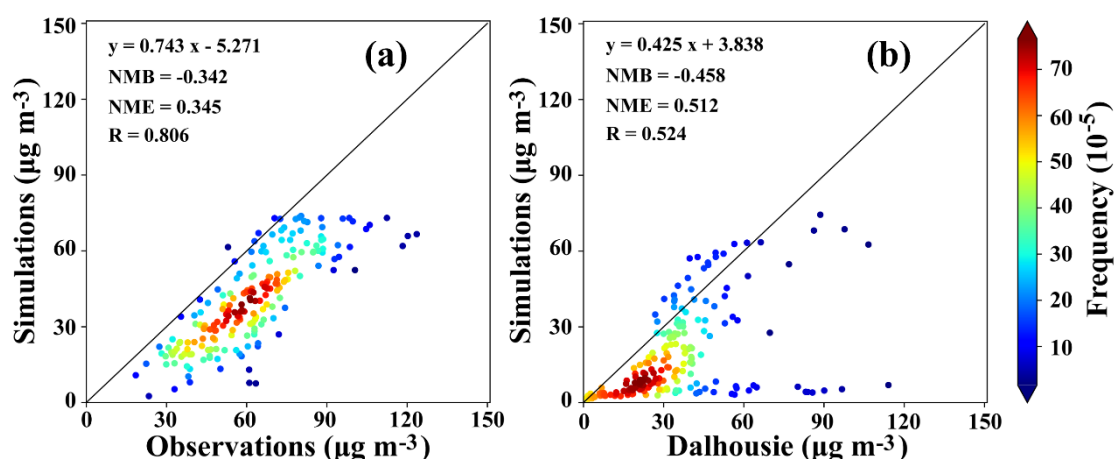
Figure 3. Density scatterplots of model performance and validation for China in scenario C$_1$ based on (a) annual mean PM$_{2.5}$ observations from MEE and (b) annual mean PM$_{2.5}$ derived from the Dalhousie dataset in 2014.

325   To verify the spatial accuracy, a comparison of the spatial distribution of simulated and observed PM$_{2.5}$,

both from MEE and Dalhousie, was conducted. Figure 4 showed the spatial distribution of the annual

mean simulated minus annual mean observed values (denoted as $diff_{si-ob}$) (Figure 4a), as well as the

spatial distribution of the annual mean simulated values minus the Dalhousie dataset (denoted as

$diff_{si-DH}$) (Figure 4b). Both Figure 4a and Figure 4b indicated that the majority of regions (central and

330   eastern China) exhibited differences ranging from -18 $\mu g\ m^{-3}$ to 0 $\mu g\ m^{-3}$, which is an underestimation

of 37% compared to the average annual observations. The simulated PM$_{2.5}$ concentrations in eastern,

central, northeastern, and western China were 37%, 21%, -49%, and 41% lower than the observations,

respectively; the simulated values were 28%, 3%, 54%, and 48% higher than the Dalhousie dataset,

respectively. The disparities in model performance across regions may be attributed to uncertainties in

335   the simulation of meteorological fields, coupled with insufficient consideration of species in the reaction

processes within the model. Considering the existing literature (Huang et al., 2021; Jia et al., 2021), it

is known that bias within approximately 50% is acceptable. For example, the PM$_{2.5}$ concentrations in

East China in 2014 simulated by Jia et al. (2021) was overestimated by 48%. Shi et al. (2021) also

reported PM$_{2.5}$ concentrations being overestimated or underestimated by 40% compared to observed

340   values. Hence, the simulated bias in this study falls within an acceptable range, meeting the research

requirements.
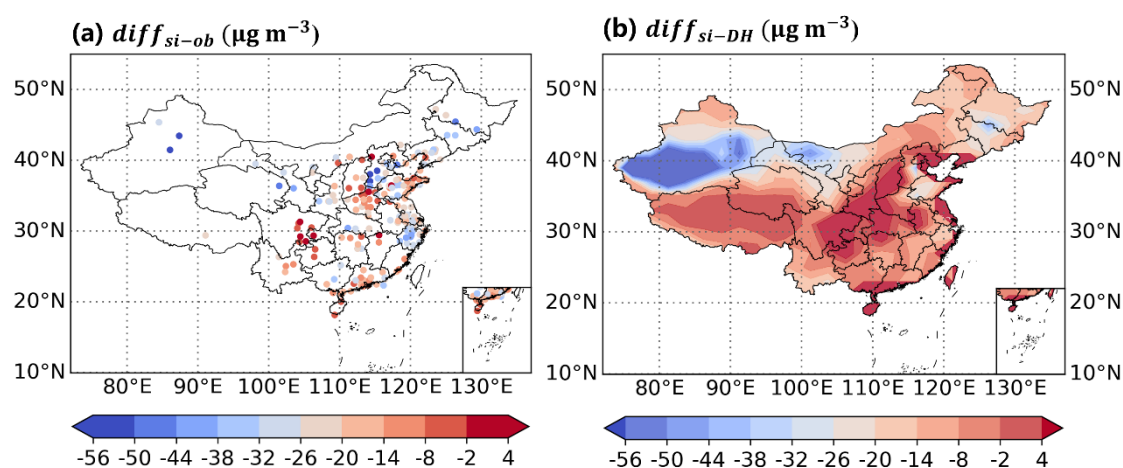
Figure 4. Spatial distribution of the annual mean simulated minus annual mean observed values (a), as well as the spatial distribution of the annual mean simulated values minus the Dalhousie dataset (b) for China in 2014 under scenario C₁.

Similarly, the model performance over time scales was also investigated. Scatter density plots and

distribution characteristics of monthly average observations and simulations for all monitoring sites in

2014 were depicted in Figure S1 and Figure 5, respectively. From Figure 5, it can be observed that the simulated values closely align with the observed values from April to September. However, in other

350 months, there was a slightly poorer alignment between simulated and observed values. Nonetheless, considering the overall performance throughout the year, as analyzed in conjunction with Figure S1, it can be deduced that both the correlation R and NME met the performance criteria suggested by Emery et al. (2017) for all months except December. Furthermore, the results in Figure 4 indicated that the bias across various regions in DEHM is acceptable. Consequently, on an aggregate level for China, the model

355 demonstrates acceptable performance in simulating monthly average $PM_{2.5}$ concentrations.
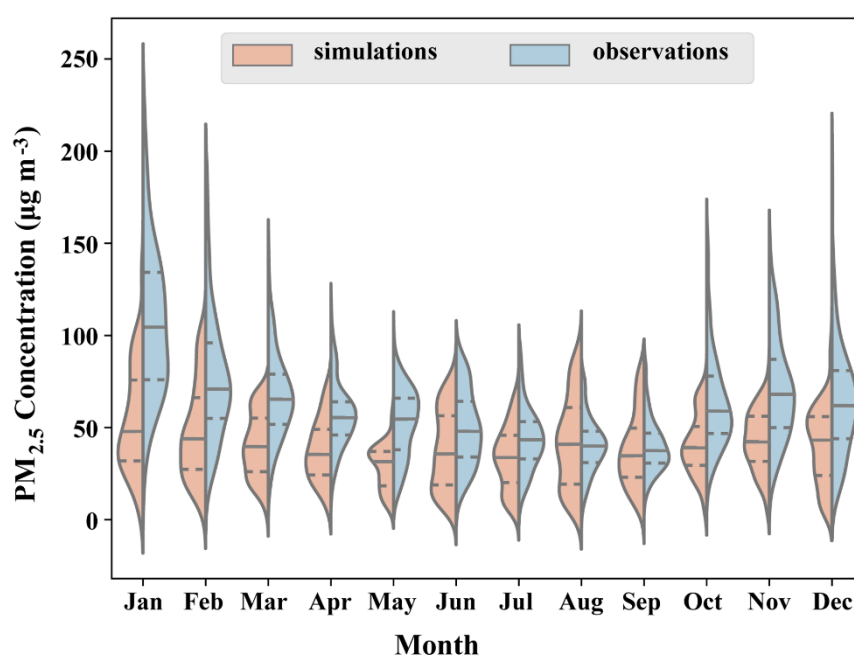
Figure 5. Violin plots of monthly average from MEE observations and simulations averaged over various observation stations for China in 2014 under scenario C_1; The red and blue colors represent the statistical distribution of simulated and observations, respectively; The width of the violin represents the sample size;

360 **The solid black line inside the violin indicates the median. The upper and lower dashed black lines within the violin indicate the upper quartile (the 75th percentile) and lower quartile (the 25th percentile), respectively.**

3.2 Spatial distribution characteristics of $PM_{2.5}$ and OP

To learn about the spatial distributions of $PM_{2.5}$ concentrations and OP, we plot maps of surface $PM_{2.5}$ and OP for scenario C_1 (Figure 6a and 6b) and quantified the average annual $PM_{2.5}$ concentrations and

365 OP across different regions of China (Figure 6c). Figure 6d depicted the geographical location of the study area. High $PM_{2.5}$ concentrations and High OP are mainly located in central and eastern urban clusters. Low $PM_{2.5}$ concentrations and Low OP are mainly distributed in northeastern and western China.

The results in Figure 6c indicated that the annual average $PM_{2.5}$ concentrations/OP in eastern, central, northeastern, and western China are 33 $\mu g\ m^{-3}$ /1.4 $nmol\ min^{-1}\ m^{-3}$, 46 $\mu g\ m^{-3}$ /2.0 $nmol\ min^{-1}\ m^{-3}$, 19 $\mu g\ m^{-3}$ /0.8 $nmol\ min^{-1}\ m^{-3}$, and 12 $\mu g\ m^{-3}$ /0.5 $nmol\ min^{-1}\ m^{-3}$, respectively.

Due to differences in city types, pollutant emission intensities, and pollutant chemical components in different regions, there are significant spatial heterogeneity in $PM_{2.5}$ concentrations and therefore in OP (see Sect. 3.4 and Figure 11 for details). Due to high population density, socio-economic activities and winter heating needs, large amounts of anthropogenic emissions, especially from industry, transportation, coal burning and biomass burning, exacerbate $PM_{2.5}$ and redox active component pollution.
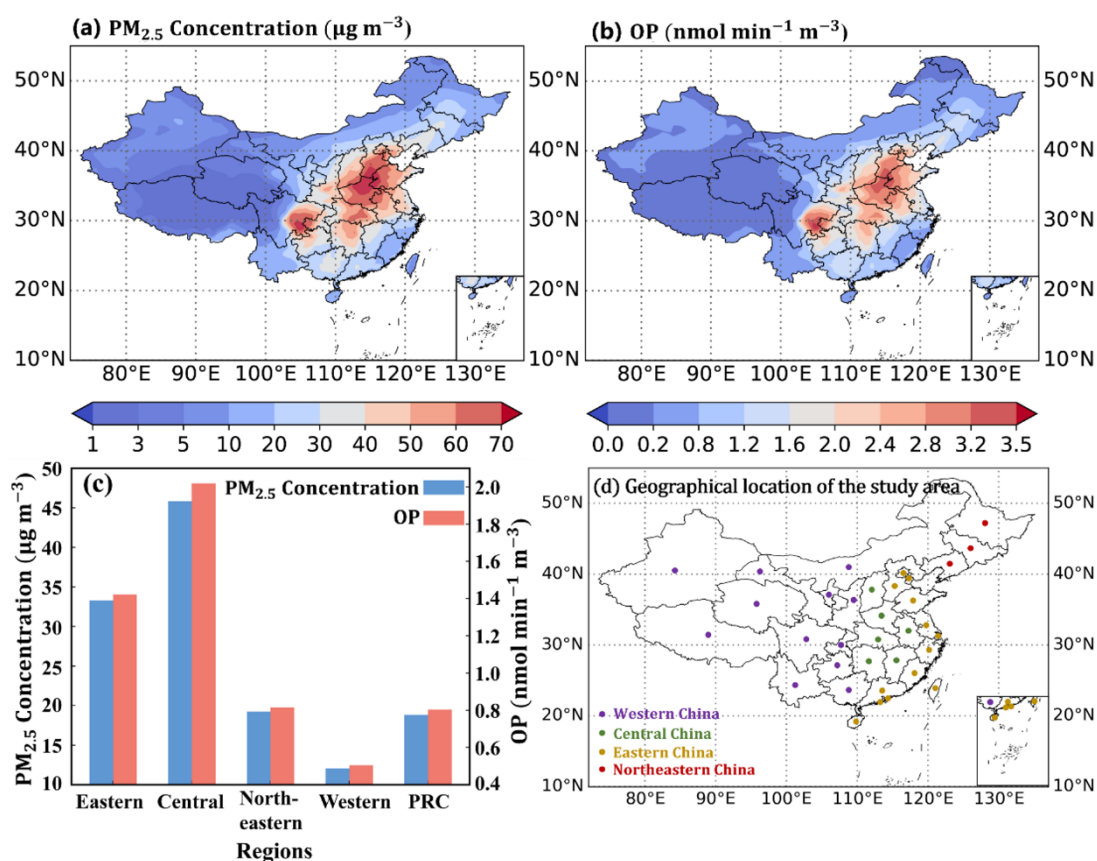
Figure 6. Spatial clustering of annual mean $PM_{2.5}$ concentrations (a) and annual mean OP (b) in China, annual mean $PM_{2.5}$ concentrations and annual mean OP (c) in different regions of China in 2014 under scenario C_1, and geographical location of the study area (d); the central region of China comprises Shanxi, Anhui, Jiangxi, Henan, Hubei, and Hunan provinces; the eastern region of China comprises Beijing, Tianjin, Hebei, Shanghai, Jiangsu, Zhejiang, Fujian, Shandong, Guangdong, Hainan, Hong Kong, Macao, and Taiwan; It should be noted that the eastern region in this study includes Hong Kong, Macao and Taiwan; the western region of China consists of twelve provinces (autonomous regions and municipalities): Inner Mongolia, Guangxi, Chongqing, Sichuan, Guizhou, Yunnan, Tibet, Shaanxi, Gansu, Qinghai, Ningxia and Xinjiang; the northeastern region of China comprises Liaoning, Jilin and Heilongjiang provinces.

To quantitatively analyze the regional distribution characteristics of $PM_{2.5}$ concentrations and OP in China, we determined the distribution function that is suitable for a specific dataset (Table 3), investigated the frequency histogram (FH) of $PM_{2.5}$ concentrations and OP, fitted the PDF, and then obtained the cumulative distribution function (CDF) by integrating PDF, as shown in Figure 7. It was found that the gamma distribution performed the best in fitting $PM_{2.5}$ concentrations and OP from Table 2. Considering the test results, the gamma distribution was used to explore the spatial distribution characteristics of $PM_{2.5}$ concentrations and OP. Figure 7a depicted the probability distribution of $PM_{2.5}$ concentrations, while Figure 7b depicted the probability distribution of OP. The wide distribution interval indicated that both $PM_{2.5}$ concentrations and OP have a similar and large spatial heterogeneity. According to the FH, the highest frequency density of $PM_{2.5}$ concentrations ranges from 10.5 to 12.9 $\mu g\ m^{-3}$; The maximum frequency density of OP ranges from 0.26 to 0.34 $nmol\ min^{-1}\ m^{-3}$. This reflects the overall pollution levels of $PM_{2.5}$ and OP in the Chinese region. Taking into account the annual average $PM_{2.5}$ concentrations limits set out in China's ambient air quality standard (AAQS, 2012), we focused on primary (15 $\mu g\ m^{-3}$) and secondary concentrations (35 $\mu g\ m^{-3}$) limits. The PDF and CDF results showed that 85% of the total area was above the primary concentrations limit and 40% was above the secondary concentrations limit. In addition, 36% of regions in China have an OP below 1.00 $nmol\ min^{-1}\ m^{-3}$, 41% have an OP between 1.00 and 2.00 $nmol\ min^{-1}\ m^{-3}$, and 23% have an OP above 2.00 $nmol\ min^{-1}\ m^{-3}$.

Table 2. Goodness-of-fit test results for China in 2014 under scenario C_1.

Item	goodness-of-fit test	Gamma	Lognormal	Exponential
$PM_{2.5}$	SSE	0.002	0.023	0.003
concentrations	KS_pvalue	0.329	0.000	0.000
OP	Sumsquare_error	0.654	0.746	1.209
	KS_pvalue	0.231	0.271	0.000

Bold values indicate the best results.

*Note:

SSE is Sum of Squared Error

KS_pvalue is the P-value of the Kolmogorov-Smirnov test
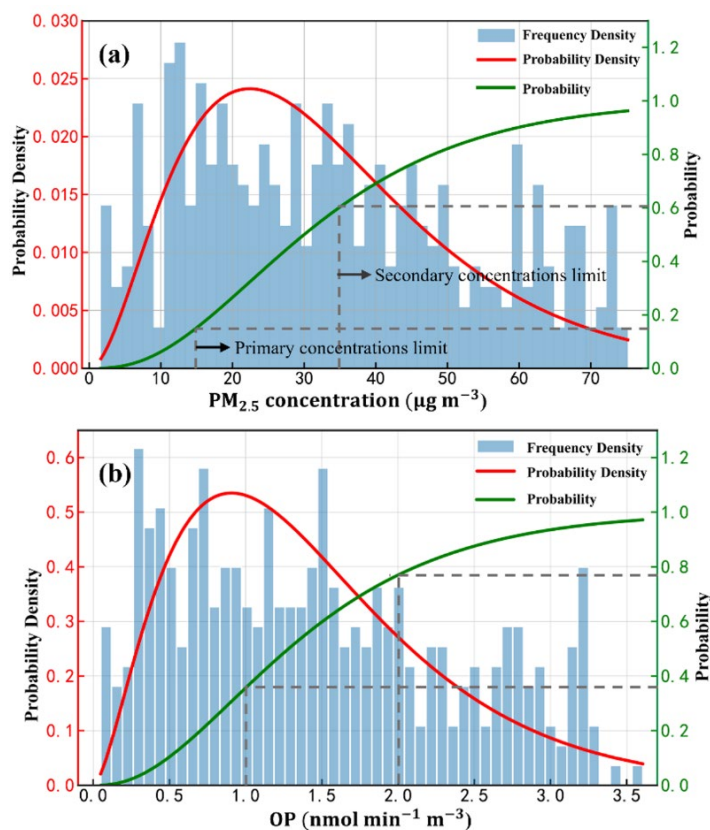
410 **Figure 7. Probability distribution of (a) annual mean PM₂.₅ concentrations and (b) annual mean OP for China in 2014 under scenario C₁.**

3.3 Contributions of meteorological conditions and emission inventories to the variations in PM$_{2.5}$ and OP

To determine the sensitivity of PM$_{2.5}$ pollution and oxidation potential (OP) to meteorological conditions (emission inventories), this study compared scenarios C$_2$ and C$_3$ (C$_1$) and investigated the impacts and contributions due to ERA5 and CESM (HTAP and Eclipse V6 emission inventories) on PM$_{2.5}$ and OP. Figure 8 illustrates the spatial distribution maps of PM$_{2.5}$ concentrations and OP under scenarios C$_1$, C$_2$, and C$_3$. Figure 9a presents the annual average PM$_{2.5}$ concentrations and OP under different scenarios, and Figure 9b shows the relative contributions of meteorological conditions and emission inventories.

From Figures 8 and 9, it can be observed that, compared to scenario C$_2$, PM$_{2.5}$ concentrations and OP are lower in the western region and slightly higher in some eastern areas under scenario C$_1$, primarily due to changes in emission inventories attributed to the inclusion or exclusion of specific local sources during the compilation process. Compared to scenario C$_3$, PM$_{2.5}$ concentrations and OP are lower in the western region and higher in some eastern areas under scenario C$_2$, primarily attributed to meteorological contributions. For the entire China region, the transition in emission inventories from Eclipse V6 to

HTAP resulted in an overall decrease in PM$_{2.5}$ concentrations of 1.55 $\mu g \, m^{-3}$, approximately 7.61%, and a decrease in OP of 0.0339 $nmol \, min^{-1} \, m^{-3}$, approximately 4.05%. The shift in meteorological data from CESM to ERA5 led to an increase in PM$_{2.5}$ concentrations of 1.22 $\mu g \, m^{-3}$, approximately 6.4%, and an increase in OP of 0.0585 $nmol \, min^{-1} \, m^{-3}$, approximately 7.5%. According to the normalization process using Equations (4)~(5), meteorological conditions contributed approximately 45.6% to the variations in PM$_{2.5}$ and approximately 65.0% to the variations in OP. Meanwhile, emission inventories contributed approximately 54.4% to the variations in PM$_{2.5}$ and approximately 35.0% to the variations in OP. Our findings highlight the significance of the quality of model input data, including emission inventories and meteorological data, for model performance.
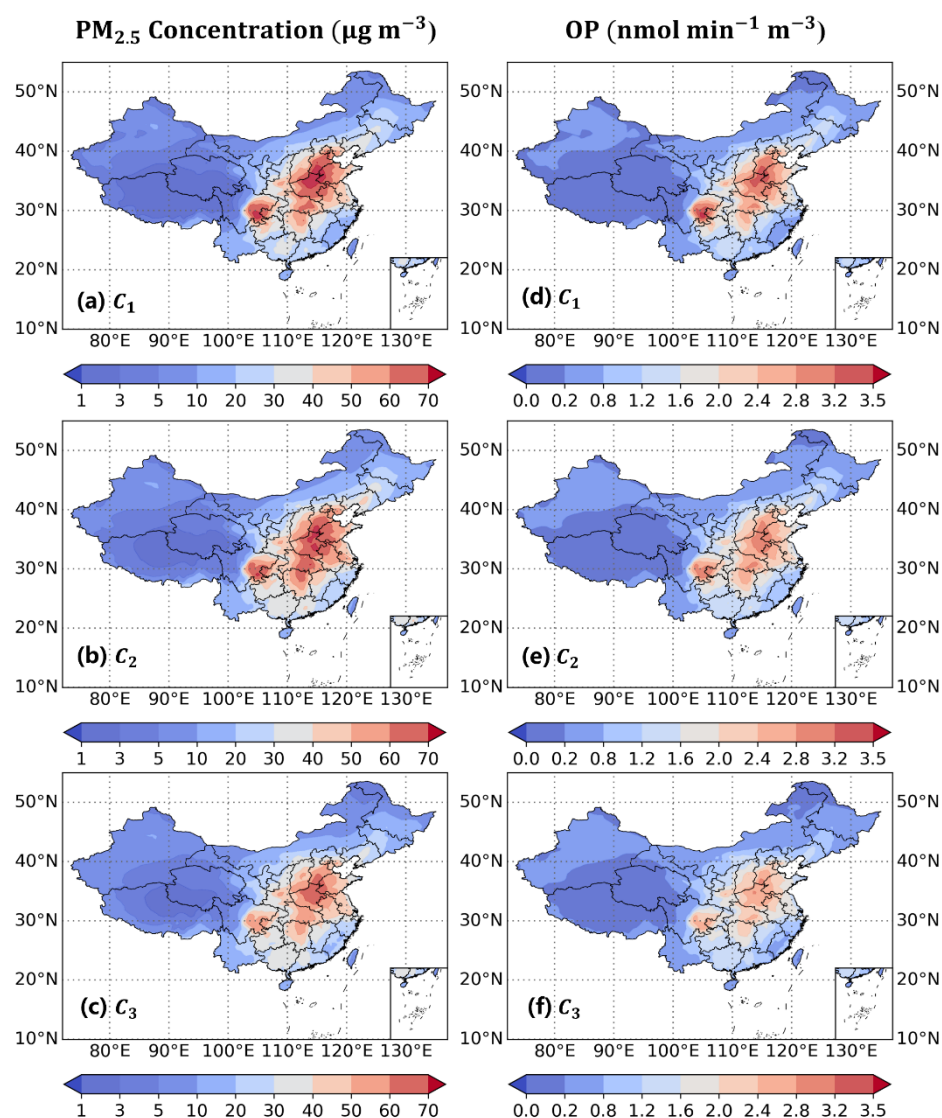
Figure 8. Spatial distribution of annual mean PM$_{2.5}$ concentrations and annual mean OP for China in 2014 under different scenarios; (a)~(c) are PM$_{2.5}$ concentrations in scenarios C$_1$, C$_2$ and C$_3$, respectively; (d)~(f) is the OP in scenarios C$_1$, C$_2$, and C$_3$, respectively; The meteorological datasets (emission inventories) employed

for scenarios C₁, C₂, and C₃ are ERA5 (EDGAR-HTAP), ERA5 (Eclipse V6), and CESM (Eclipse V6),
respectively.
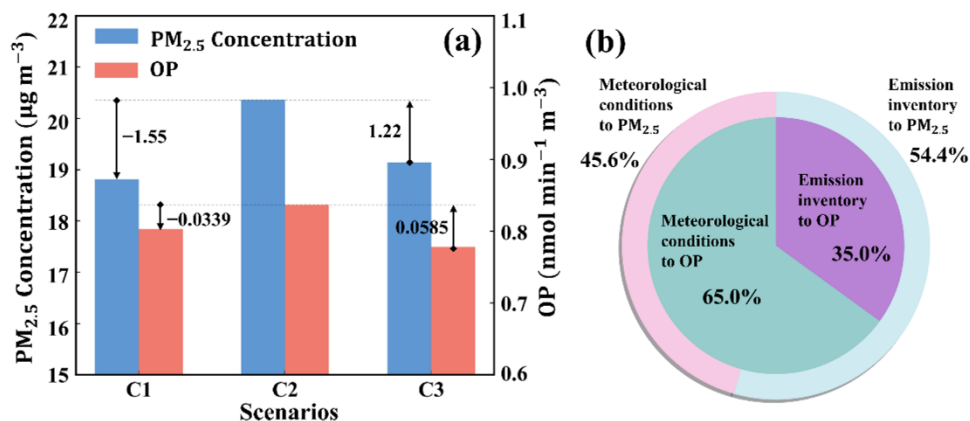
Figure 9. (a) Average annual PM₂.₅ concentrations and Average annual OP for China in 2014 under different
scenarios; (b) The relative contribution of meteorological conditions and emission inventories to Average
annual PM₂.₅ and Average annual OP for China in 2014, with the outer circle representing PM₂.₅ and the
inner circle representing OP; The meteorological datasets (emission inventories) employed for scenarios C₁,
C₂, and C₃ are ERA5 (EDGAR-HTAP), ERA5 (Eclipse V6), and CESM (Eclipse V6), respectively.

3.4 Contribution of anthropogenic emission sources to PM₂.₅ and OP

To determine the impact of anthropogenic emissions on PM₂.₅ and OP, we quantified their percent
contribution (Figure 10). Secondary aerosol formation, biomass burning, industrial, coal combustion for
residential heating, and transportation sources contributed 48%, 21%, 21%, 6% and 4% to PM₂.₅,
respectively. Secondary aerosol formation, biomass burning, coal combustion for residential heating,
industrial sources, and transportation sources contributed 58%, 21%, 11%, 9% and 1% to OP,
respectively. This means that secondary aerosol formation and biomass burning are the main sources of
PM₂.₅ and OP.
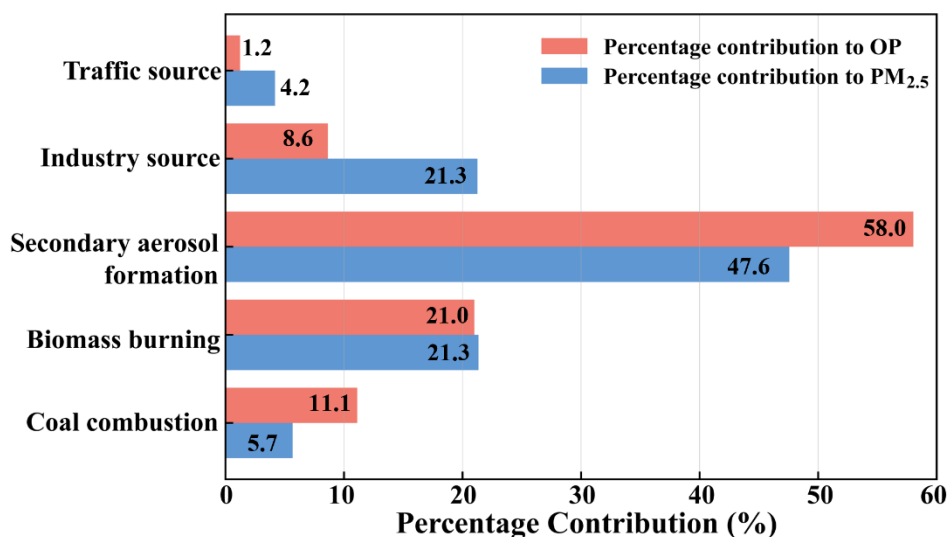
Figure 10. Percentage contribution of different anthropogenic sources (coal combustion for residential heating, biomass burning, secondary aerosol formation, industry, and traffic) to total PM$_{2.5}$ concentrations and OP for China in 2014 under scenario C$_1$.

Thus, we explored the spatial distribution characteristics of PM$_{2.5}$ and OP from different anthropogenic sources to reveal the spatial contributions of PM$_{2.5}$ concentrations and OP, as shown in Figure 11. It was observed that the spatial distribution features of PM$_{2.5}$ concentrations and OP from each emission source are similar to those in Figure 6, and they all adhere to the principle that the eastern region is higher than the western.

It can be seen from Figure 11 that the main reason that secondary aerosol formation is the main anthropogenic source of both PM$_{2.5}$ concentrations and OP in China is due to the higher pollution levels, more contributions to mass, and toxicity in the central and eastern regions. Relevant study (Molina et al., 2023) has highlighted the significant contribution of secondary aerosol formation to particle mass and intrinsic OP.

Due to Chinese crops, especially corn straw, and power plants are mainly concentrated in central and eastern regions, northeast and part of the western region, as well as the bigger intrinsic OP (Equation (1)), this results in biomass burning becoming the second contribution.

In this study, coal combustion refers to coal heating from the residential sector. Coal burning increases secondary inorganic and organic aerosols in the air (Liu et al., 2018) which leads to stronger oxidative toxicity. Thus, due to greater heating demand in locations with high population density and chilly winters (e.g., the northern part of the central and eastern China), PM$_{2.5}$ concentrations and OP linked to coal burning are higher.

Industrial emissions are mainly derived from specific industrial processes in the iron and steel industrial base, metallurgical production plants for non-ferrous metals (e.g., titanium and molybdenum), and so on. This is one main source for metals. Due to the correlation between these transition metals and OP (Fang et al., 2017; Liu et al., 2018), China's four industrial zones (Liaozhong-South Heavy Industry Base, Beijing-Tianjin-Tangshan Industrial Base, Shanghai-Nanjing-Hangzhou Industrial Base, and Pearl River Delta Light Industry Base) are important contributors to PM$_{2.5}$ and OP emissions from industrial sources. The transportation sector in the DEHM model only considers tailpipe emissions, excluding non-exhaust emissions from vehicles like road dust, brake dust, and tire wear, which is a main reason that the traffic sources exhibit the lowest contribution to PM$_{2.5}$ concentrations/OP. Moreover, it can be observed from

Figure 11 that the sector's emissions are mainly concentrated in a small number of regions, such as Henan,

Hebei, and Shandong. This is valid for the top three provinces in terms of vehicle particulate matter and

nitrogen oxide emissions in 2014 according to China Annual Vehicle Pollution Prevention and Control

Report (MEE, 2015).

490
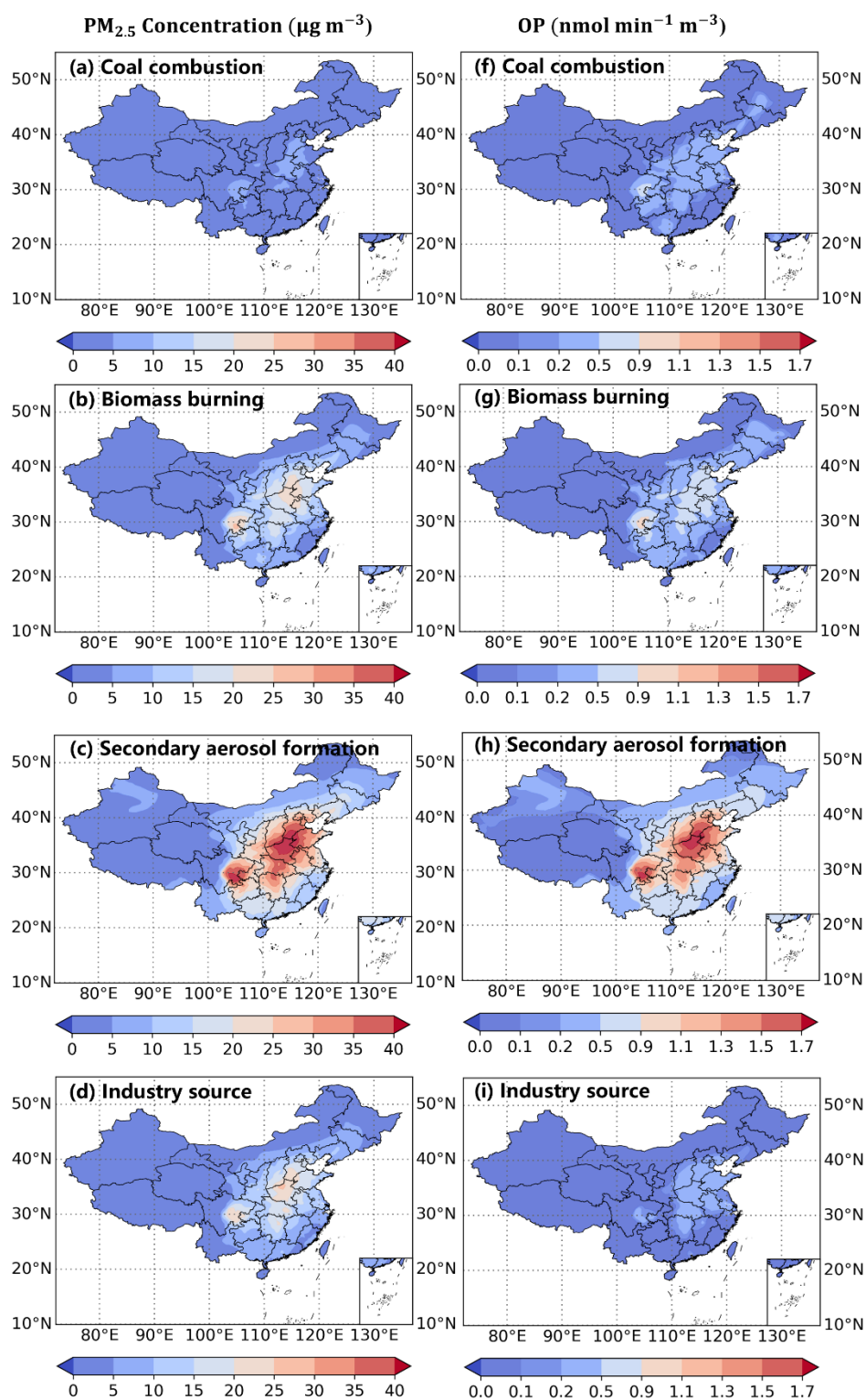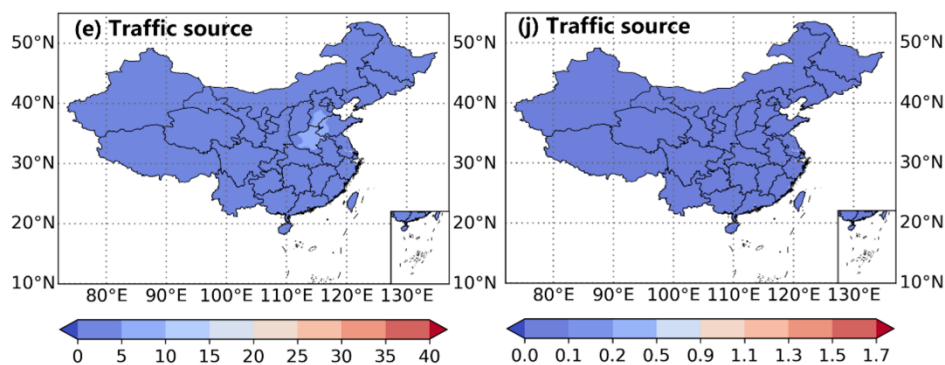
Figure 11. Spatial distribution of annual mean PM$_{2.5}$ concentrations and annual mean OP from different anthropogenic sources for China in 2014 under scenario C$_1$; (a)~(e) are PM$_{2.5}$ concentrations derived from coal combustion for residential heating, biomass burning, secondary aerosol formation, industry, and traffic respectively; (f)~(j) are the OP derived from coal combustion for residential heating, biomass burning, secondary aerosol formation, industry, and traffic respectively.

3.5 Uncertainty of OP estimates

OP is considered an important indicator of PM$_{2.5}$ toxicity and is associated with adverse health effects. Linking the predicted health effects of aerosols to OP may be more relevant than considering PM$_{2.5}$ mass alone (Alwadei et al., 2020). However, previous studies of OP in China have mainly focused on local areas, and OP and its source are very different in space and time (Wen et al., 2023), which makes the health research of OP challenging. At present, there are two kinds of methods for evaluating OP of PM$_{2.5}$: cellular method and non-cellular method. The reproducibility of cellular methods is poor, and it is difficult to achieve a large sample size analysis. And the choice of cell type or cell line can significantly affect the OP results (Xing et al., 2023). The non-cellular method has the advantages of fast speed, simple operation, high reproducibility, and low cost. The most common non-cellular methods are DTT, AA, GSH, and 2', 7' -dichlorofluorescein (DCFH) assays (Pietrogrande et al., 2019). However, standardized experimental methods for evaluating OP have not been established (Song et al., 2021), and it is difficult to provide more consistent data on OP across samples at different locations and times. Moreover, each non-cellular OP assay is specific for ROS, making none of the methods used as a standard method for assessing the toxicity of environmental particles. Several studies have used a multi-measure approach to compensate for the specificity of a single probe response to ROS (Calas et al., 2018; Puthussery et al., 2020; Yu et al., 2021; Xu et al., 2021). Xu et al. (2021) used three measurement methods (OP^{DTT}, OP^{AA}, and OP^{GSH}) to estimate the Canadian annual mean OP and found that the sensitivity of the three methods to different components varied widely. Choosing a variety of methods

for OP measurement can lead to more comprehensive results, but it can also lead to a significant increase in workload.

520   For this, we propose a hybrid approach combining existing observations of OP with the CTM. So, using OP from assays and their observed links to sources and chemical constituents can then be parameterized and implemented in CTM for a comprehensive assessment of OP exposure over large areas and time periods. The method considers the seasonal characteristics of the chemical composition of $PM_{2.5}$ and the DTT activity measurement of $PM_{2.5}$. A positive matrix factorization (PMF) model and multiple linear

525   regression (MLR) model were used to quantify the contribution of $PM_{2.5}$ emission sources to OP (the volume-normalized DTT activity, DTT_v). The normalized regression equation in this study provides the sensitivity of OP to each identified source. The advantage is that directly applying predicted and readily available $PM_{2.5}$ data makes it easy to estimate the OP and assess health risks over large regions and across time and space. This approach enables the exploration of spatial and seasonal variations in aerosol OP

530   across China, providing insight into the contribution of sources, atmospheric processes, and meteorological conditions. There are some main limitations to this study that may lead to uncertainty in predicting OP outcomes. Firstly, the OP prediction considered is incomplete and does not include all sources of OP. For example, the transportation sector refers only to road transport, excluding emissions from ships and other mobile sources. And the transportation sector only considers tailpipe emissions in

535   traffic. These lead to some OP uncertainties. Additionally, this study only considers the intrinsic OP of total SOA due to limited long-term measurements of SOA. Different types of SOA may exhibit varied OP responses due to differences in their sources, formation pathways, and chemical compositions. Aging and fresh SOA may also exhibit varying toxicities (Liu et al., 2023). In future research, efforts should be made to comprehensively collect $PM_{2.5}$ samples from various sources and fully explore the potential

540   relationships between OP and $PM_{2.5}$ components/sources to further improve OP prediction models and reduce prediction uncertainties. Secondly, the OP prediction model adopted in this paper is based on Liu et al. (2018). The data samples are from DTT experimental measurements conducted in various coastal cities and from different emission sources, with limited data samples. In this study, it is used to predict the OP of cities across the country, which inevitably leads to a slight error in the forecast results. However,

545   due to the spatiotemporal and emission source differences of the data samples were considered, the three cities selected are representative, which reduces the errors caused by the data samples to a certain extent. Thirdly, a significant body of literature also indicates that vertical resolution can reflect atmospheric

thermodynamic environments and the evolution processes of mesoscale systems, which are related to the diffusion and transport of $PM_{2.5}$. Insufficient vertical resolution can hinder the accurate prediction of

550     $PM_{2.5}$ surface concentrations (HARA, 2011; Li et al., 2022; Li et al., 2023). Therefore, the configuration of the DEHM model (e.g., vertical resolution) also introduces uncertainties to this study. In conclusion, the results calculated by the method proposed in this study are compared with the existing measurement data (Liu et al., 2014; Liu et al., 2018; Wang et al., 2019), and a good agreement is observed. For instance, through DTT measurements, Zhang et al. (2023) reported an average OP^{DTTv} of 1.33

555     $nmol\ min^{-1}\ m^{-3}$ from January 2020 to June 2021 in downtown Nanjing, located in the YRD region of China, with a range of 0.82~2.08 $nmol\ min^{-1}\ m^{-3}$. This is close to our estimated results (Liu et al., 2024) for the YRD region, where the annual mean OP during 2010-2014 was 1.56 $nmol\ min^{-1}\ m^{-3}$, and the annual mean OP for 2020 under two emission reduction scenarios were 1.36 $nmol\ min^{-1}\ m^{-3}$ and 1.25 $nmol\ min^{-1}\ m^{-3}$, respectively. The relative errors for the two scenarios

560   were 2.3% and 6.0%. Another study (Liu et al., 2020) investigating the OP of $PM_{2.5}$ in Wuhan, located in the CC region, reported a mean OP^{DTTv} of 1.8 $nmol\ min^{-1}\ m^{-3}$ for the summer of 2012 in downtown Wuhan. This aligns closely with our estimated results (Liu et al., 2024) for the CC region (1.73 $nmol\ min^{-1}\ m^{-3}$), with a relative error of 3.9%. Therefore, the method proposed in this study is reliable. The proposed method provides a possibility to solve the difficulty and high cost of OP measurement.

565   **4. Conclusions**

This study established a spatial modelling for $PM_{2.5}$ concentrations and OP, provided a method for calculating OP across China, and quantitatively assessed the impacts of meteorological conditions and anthropogenic emissions on $PM_{2.5}$ and OP variability and levels in China. The following conclusions can be obtained:

570   • $PM_{2.5}$ and OP exhibited spatial clustering characteristics, with higher values mainly located in the central and eastern urban areas. About 85% and 40% of the areas had $PM_{2.5}$ annual average concentrations exceeding the first-grade concentrations limit (15 $\mu g\ m^{-3}$) and second-grade concentrations limit (35 $\mu g\ m^{-3}$), respectively. Additionally, about 36% of the areas had OP concentrations lower than 1 $nmol\ min^{-1}\ m^{-3}$, while 23% of the areas had OP concentrations

575   higher than 2 $nmol\ min^{-1}\ m^{-3}$.

- Variability in both $PM_{2.5}$ and OP are influenced by a combination of meteorological conditions and emission inventories. Meteorological conditions contributed about 46% of $PM_{2.5}$ variation and 65% of OP variation. The emission inventory contributed about 54% of the change in $PM_{2.5}$ and about 35% of the change in OP.

580
- The percentage contributions of secondary aerosol formation, biomass burning, industry, coal combustion for residential heating, and traffic to $PM_{2.5}$ were about 48%, 21%, 21%, 6%, and 4%, respectively. The percentage contributions of secondary aerosol formation, biomass burning, coal combustion for residential heating, industry, and traffic to OP were approximately 58%, 21%, 11%, 9%, and 1%, respectively.

585 A main finding of this study is that meteorological variability is the prime driver of OP variability, and not emissions. Furthermore, secondary aerosol formation and biomass burning are the main sources of OP. Thus, air pollution strategies should focus more on biomass burning and the emissions of the precursors taking part in the secondary aerosol formation, and it would be efficient to introduce special emissions controls during stagnation or other periods where OP accumulates.

590

Author contributions

Jiemei Liu performed the simulation and its validation, data analysis, investigation, and writing – original draft. Jesper H. Christensen conducted investigation, worked on methodology, and performed validation. Zhuyun Ye conducted investigation, data analysis, worked on methodology. Shikui Dong provided the suggestion of data analysis, and manuscript feedback. Camilla Geels conducted investigation and provided the suggestion of simulation. Jørgen Brandt conducted investigation. Athanasios Nenes conducted investigation and provided manuscript feedback. Yuan Yuan provided manuscript feedback, supervision, provided acquired funding. Ulas Im provided the resources, supervised this work, provided manuscript feedback, and managed the project administration. All authors discussed the results and commented on the manuscript.

Competing interests

The contact author has declared that none of the authors has any competing interests.

Acknowledgements:

This study was supported by the National Natural Science Foundation of China (Grant No. 52041601). The work of Liu Jiemei was also supported by China Scholarship Council (CSC) under the State Scholarship Fund. AN acknowledges support from the project PyroTRACH (ERC-2016-COG) funded from H2020-EU.1.1. - Excellent Science - European Research Council (ERC), project ID 726165 and from the European Union project EASVOLEE funded from HORIZON-CL5-2022-D5-01 (project ID 101095457).

Declaration of conflicting interests:

The authors declare no conflicts of interests.

Supplement:

Density scatterplots of model performance and validation based on monthly mean observations (Figure S1) is provided in the Supplementary Materials file.

References:

AAQS. (2012). National standard of the People's Republic of China GB3095-2012. https://www.mee.gov.cn/ywgz/fgbz/bz/bzwb/dqhjbh/dqhjzlbz/201203/W0201204103302323 98521.pdf. Accessed 11 January, 2023.

Ainur, D., Chen, Q., Sha, T., Zarak, M., Dong, Z., Guo, W., Zhang, Z., Dina, K., An, T. (2023). Outdoor Health Risk of Atmospheric Particulate Matter at Night in Xi'an, Northwestern China. *Environ Sci Technol*, 57, 9252-9265. https://doi.org/10.1021/acs.est.3c02670.

Alexandratos, N., Bruinsma, J., 2012. World agriculture towards 2030/2050, the 2012 revision (No. No. 12-03), ESA Working Paper. World Food and Agricultural Organization, Rome, Italy.

Alwadei, M., Thomson, S., Kramer, L., Shi, Z., Bloss, W., (2020). Oxidative Potential of PM2. 5 in Dammam, Saudi Arabia, and the effect of dust storms.

Brandt, J., Silver, J.D., Christensen, J.H., Andersen, M.S., B O Nl O Kke, J.H., Sigsgaard, T., Geels, C., Gross, A., Hansen, A.B., Hansen, K.M., Hedegaard, G.B., Kaas, E., Frohn, L.M. (2013a). Contribution from the ten major emission sectors in Europe and Denmark to the health-cost externalities of air pollution using the EVA model system – an integrated modelling approach. *Atmos Chem Phys*, 13, 7725-7746. https://doi.org/10.5194/acp-13-7725-2013.

Brandt, J., Silver, J.D., Christensen, J.H., Andersen, M.S., B O Nl O Kke, J.H., Sigsgaard, T., Geels, C., Gross, A., Hansen, A.B., Hansen, K.M., Hedegaard, G.B., Kaas, E., Frohn, L.M. (2013b). Assessment of past, present and future health-cost externalities of air pollution in Europe and the contribution from international ship traffic using the EVA model system. *Atmos Chem Phys*, 13, 7747-7764. https://doi.org/10.5194/acp-13-7747-2013.

Brandt, J., Silver, J.D., Frohn, L.M., Geels, C., Gross, A., Hansen, A.B., Hansen, K.M., Hedegaard, G.B., Skjøth, C.A., Villadsen, H., Zare, A., Christensen, J.H. (2012). An integrated model study for Europe and North America using the Danish Eulerian Hemispheric Model with focus on intercontinental transport of air pollution. *Atmos Environ (1994)*, 53, 156-176. https://doi.org/10.1016/j.atmosenv.2012.01.011.

Calas, A., Uzu, G., Kelly, F.J., Houdier, S., Martins, J.M.F., Thomas, F., Molton, F., Charron, A., Dunster, C., Oliete, A., Jacob, V., Besombes, J.L., Chevrier, F., Jaffrezo, J.L. (2018). Comparison between five acellular oxidative potential measurement assays performed with detailed chemistry on PM10 samples from the city of Chamonix (France). *Atmos Chem Phys*, 18, 7863-7875. https://doi.org/10.5194/acp-18-7863-2018.

Campbell, S.J., Wolfer, K., Utinger, B., Westwood, J., Zhang, Z.H., Bukowiecki, N., Steimer, S.S., Vu, T.V., Xu, J.S., Straw, N., Thomson, S., Elzein, A., Sun, Y.L., Liu, D., Li, L.J., Fu, P.Q., Lewis, A.C., Harrison, R.M., Bloss, W.J., Loh, M., Miller, M.R., Shi, Z.B., Kalberer, M. (2021). Atmospheric conditions and composition that influence PM2.5 oxidative potential in Beijing, China. *Atmos Chem Phys*, 21, 5549-5573. https://doi.org/10.5194/acp-21-5549-2021.

CESM. (2023). Community Earth System Model. https://www.cesm.ucar.edu/. Accessed 7 May, 2023.

Chen, L., Wang, T., Bo, X., Zhuang, Z., Qu, J., Xue, X., Tian, J., Huang, M., Wang, P., Sang, M. (2022). Thermal Power Industry Emissions and Their Contribution to Air Quality on the Fen-

Wei Plain. *Atmosphere (Basel)*, 13. https://doi.org/10.3390/atmos13050652.

Chen, P., Wang, T., Kasoar, M., Xie, M., Li, S., Zhuang, B., Li, M. (2018). Source Apportionment of PM2.5 during Haze and Non-Haze Episodes in Wuxi, China. *Atmosphere (Basel)*, 9, 267. https://doi.org/10.3390/atmos9070267.

665   Chen, T., Cao, S. (2021). Numerical study on the integrated effects of supplied air velocity and exhaust velocity on particles removal for industrial buildings. *Energy and Built Environment*, 2, 380-391. https://doi.org/10.1016/j.enbenv.2020.09.006.

Chen, T., Cao, S., Wang, J., Nizamani, A.G., Feng, Z., Kumar, P. (2021). Influences of the optimized air curtain at subway entrance to reduce the ingress of outdoor airborne particles.

670   *Energy Build*, 244, 111028. https://doi.org/10.1016/j.enbuild.2021.111028.

Chen, Z.Y., Chen, D.L., Kwan, M.P., Chen, B., Gao, B.B., Zhuang, Y., Li, R.Y., Xu, B. (2019). The control of anthropogenic emissions contributed to 80% of the decrease in PM2.5 concentrations in Beijing from 2013 to 2017. *Atmos Chem Phys*, 19, 13519-13533. https://doi.org/10.5194/acp-19-13519-2019.

675   Christensen, J.H. (1997). The Danish eulerian hemispheric model — a three-dimensional air pollution model used for the arctic. *Atmos Environ (1994)*, 31, 4169-4191. https://doi.org/10.1016/S1352-2310(97)00264-1.

Collin, G. (2020). Regional Production, Updated documentation covering all Regional operational systems and the ENSEMBLE. https://atmosphere.copernicus.eu/sites/default/files/2020-

680   01/CAMS50_2018SC1_D2.0.2-U1_Models_documentation_201910_v1.pdf. Accessed.

Cramer, J., Jorgensen, J.T., Hoffmann, B., Loft, S., Brauner, E.V., Prescott, E., Ketzel, M., Hertel, O., Brandt, J., Jensen, S.S., Backalarz, C., Simonsen, M.K., Andersen, Z.J. (2020). Long-Term Exposure to Air Pollution and Incidence of Myocardial Infarction: A Danish Nurse Cohort Study. *Environ Health Perspect*, 128. https://doi.org/10.1289/EHP5818.

685   Crippa, M., Guizzardi, D., Butler, T., Keating, T., Wu, R., Kaminski, J., Kuenen, J., Kurokawa, J., Chatani, S., Morikawa, T., Pouliot, G., Racine, J., Moran, M.D., Klimont, Z., Manseau, P.M., Mashayekhi, R., Henderson, B.H., Smith, S.J., Suchyta, H., Muntean, M., Solazzo, E., Banja, M., Schaaf, E., Pagani, F., Woo, J.H., Kim, J., Monforti-Ferrario, F., Pisoni, E., Zhang, J., Niemi, D., Sassi, M., Ansari, T., Foley, K. (2023). The HTAP_v3 emission mosaic: merging

690   regional and global monthly emissions (2000--2018) to support air quality modelling and policies. *Earth Syst Sci Data*, 15, 2667-2694. https://doi.org/10.5194/essd-15-2667-2023.

Danabasoglu, G., Lamarque, J.F., Bacmeister, J., Bailey, D.A., DuVivier, A.K., Edwards, J., Emmons, L.K., Fasullo, J., Garcia, R., Gettelman, A., Hannay, C., Holland, M.M., Large, W.G., Lauritzen, P.H., Lawrence, D.M., Lenaerts, J.T.M., Lindsay, K., Lipscomb, W.H.,

695   Mills, M.J., Neale, R., Oleson, K.W., Otto-Bliesner, B., Phillips, A.S., Sacks, W., Tilmes, S., van Kampenhout, L., Vertenstein, M., Bertini, A., Dennis, J., Deser, C., Fischer, C., Fox-Kemper, B., Kay, J.E., Kinnison, D., Kushner, P.J., Larson, V.E., Long, M.C., Mickelson, S., Moore, J.K., Nienhouse, E., Polvani, L., Rasch, P.J., Strand, W.G. (2020). The Community Earth System Model Version 2 (CESM2). *J Adv Model Earth Syst*, 12, e2019MS001916.

700   https://doi.org/10.1029/2019MS001916.

de Melo, J.E., Pellicane, P.J., de Souza, M.R. (2000). Goodness-of-fit analysis on wood properties data from six Brazilian tropical hardwoods. *Wood Sci Technol*, 34, 83-97. https://doi.org/10.1007/s002260000033.

Eclipse. (2020). Global emission fields of air pollutants and GHGs. https://iiasa.ac.at/models-

705   tools-data/global-emission-fields-of-air-pollutants-and-ghgs. Accessed 7 May, 2023.

Emery, C., Liu, Z., Russell, A.G., Odman, M.T., Yarwood, G., Kumar, N. (2017). Recommendations on statistics and benchmarks to assess photochemical model performance. *J Air Waste Manag Assoc*, 67, 582-598. https://doi-org.ez.statsbiblioteket.dk/10.1080/10962247.2016.1265027.

710   ERA. (2023). ECMWF Reanalysis v5. https://www.ecmwf.int/en/forecasts/dataset/ecmwf-reanalysis-v5. Accessed 22 May, 2023.

Fang, T., Guo, H., Zeng, L., Verma, V., Nenes, A., Weber, R.J. (2017). Highly Acidic Ambient Particles, Soluble Metals, and Oxidative Potential: A Link between Sulfate and Aerosol Toxicity. *Environ Sci Technol*, 51, 2611-2620. https://doi.org/10.1021/acs.est.6b06151.

715   Frohn, L.M., Geels, C., Andersen, C., Andersson, C., Bennet, C., Christensen, J.H., Im, U., Karvosenoja, N., Kindler, P.A., Kukkonen, J., Lopez-Aparicio, S., Nielsen, O., Palamarchuk, Y., Paunu, V., Plejdrup, M.S., Segersson, D., Sofiev, M., Brandt, J. (2022). Evaluation of multidecadal high-resolution atmospheric chemistry-transport modelling for exposure assessments in the continental Nordic countries. *Atmos Environ (1994)*, 290, 119334.

720   https://doi.org/10.1016/j.atmosenv.2022.119334.

Frost, G.J., Middleton, P., Tarrasón, L., Granier, C., Guenther, A., Cardenas, B., Denier Van Der Gon, H., Janssens-Maenhout, G., Kaiser, J.W., Keating, T., Klimont, Z., Lamarque, J., Liousse, C., Nickovic, S., Ohara, T., Schultz, M.G., Skiba, U., van Aardenne, J., Wang, Y. (2013). New Directions: GEIA's 2020 vision for better air emissions information. *Atmos*

725   *Environ (1994)*, 81, 710-712. https://doi.org/10.1016/j.atmosenv.2013.08.063.

Galmarini, S., Koffi, B., Solazzo, E., Keating, T., Hogrefe, C., Schulz, M., Benedictow, A., Griesfeller, J.J., Janssens-Maenhout, G., Carmichael, G., Fu, J., Dentener, F. (2017). Technical note: Coordination and harmonization of the multi-scale, multi-model activities HTAP2, AQMEII3, and MICS-Asia3: simulations, emission inventories, boundary

730   conditions, and model output formats. *Atmos Chem Phys*, 17, 1543-1555. https://doi.org/10.5194/acp-17-1543-2017.

Gao, D., Pollitt, K., Mulholland, J.A., Russell, A.G., Weber, R.J. (2020). Characterization and comparison of PM2.5 oxidative potential assessed by two acellular assays. *Atmos Chem Phys*, 20, 5197-5210. https://doi.org/10.5194/acp-20-5197-2020.

735   García-Martínez, I.M., Bollasina, M.A., Undorf, S. (2020). Strong large-scale climate response to North American sulphate aerosols in CESM. *Environ Res Lett*, 15, 114051. https://iopscience.iop.org/article/10.1088/1748-9326/abbe45.

Geels, C., Andersson, C., Hänninen, O., Lansø, A.S., Schwarze, P.E., Skjøth, C.A., Brandt, J. (2015). Future Premature Mortality Due to O3, Secondary Inorganic Aerosols and Primary

740   PM in Europe — Sensitivity to Changes in Climate, Anthropogenic Emissions, Population and Building Stock. *International Journal of Environmental Research and Public Health*, 12, 2837-2869. https://doi.org/10.3390/ijerph120302837.

Geels, C., Winther, M., Andersson, C., Jalkanen, J.P., Brandt, J., Frohn, L.M., Im, U., Leung, W., Christensen, J.H. (2021). Projections of shipping emissions and the related impact on air

745   pollution and human health in the Nordic region. *Atmos Chem Phys*, 21, 12495-12519. https://doi.org/10.5194/acp-21-12495-2021.

Gong, S., Zhang, L., Liu, C., Lu, S., Pan, W., Zhang, Y. (2022). Multi-scale analysis of the impacts of meteorology and emissions on PM2.5 and O3 trends at various regions in China

from 2013 to 2020 2. Key weather elements and emissions. *Sci Total Environ*, 824, 153847. https://doi.org/10.1016/j.scitotenv.2022.153847.

HARA, T. (2011). Vertical resolution dependency of boundary layer schemes. https://www.wcrp-climate.org/WGNE/BlueBook/2011/individual-articles/04_Tabito_Hara_04_hara_tabito_vertical_resolution_dependency.pdf.

Hersbach, H., Bell, B., Berrisford, P., Hirahara, S., Horányi, A., Muñoz-Sabater, J., Nicolas, J., Peubey, C., Radu, R., Schepers, D., Simmons, A., Soci, C., Abdalla, S., Abellan, X., Balsamo, G., Bechtold, P., Biavati, G., Bidlot, J., Bonavita, M., De Chiara, G., Dahlgren, P., Dee, D., Diamantakis, M., Dragani, R., Flemming, J., Forbes, R., Fuentes, M., Geer, A., Haimberger, L., Healy, S., Hogan, R.J., Hólm, E., Janisková, M., Keeley, S., Laloyaux, P., Lopez, P., Lupu, C., Radnoti, G., de Rosnay, P., Rozum, I., Vamborg, F., Villaume, S., Thépaut, J. (2020). The ERA5 global reanalysis. *Q J R Meteorol Soc*, 146, 1999-2049. https://doi.org/10.1002/qj.3803.

Hodan, W.M., Barnard, W.R. (2004). Evaluating the contribution of PM2. 5 precursor gases and re-entrained road emissions to mobile source PM2. 5 particulate matter emissions. *MACTEC Federal Programs, Research Triangle Park, NC*. https://www3.epa.gov/ttnchie1/conference/ei13/mobile/hodan.pdf.

Hong, S., Noh, Y., Dudhia, J. (2006). A New Vertical Diffusion Package with an Explicit Treatment of Entrainment Processes. *Mon Weather Rev*, 134, 2318-2341. https://doi.org/10.1175/MWR3199.1.

Huang, L., Zhu, Y., Zhai, H., Xue, S., Zhu, T., Shao, Y., Liu, Z., Emery, C., Yarwood, G., Wang, Y., Fu, J., Zhang, K., Li, L. (2021). Recommendations on benchmarks for numerical air quality model applications in China – Part 1: PM2.5 and chemical species. *Atmos Chem Phys*, 21, 2725-2743. https://doi.org/10.5194/acp-21-2725-2021.

IEA, 2011. World Energy Outlook 2011. International Energy Agency, Paris, France.

IEA, 2012. Energy Technology Perspectives. 2012 - Pathways to a Clean Energy System. OECD/IEA, International Energy Agency, Paris.

Im, U., Bauer, S.E., Frohn, L.M., Geels, C., Tsigaridis, K., Brandt, J. (2023). Present-day and future PM2.5 and O3-related global and regional premature mortality in the EVAv6.0 health impact assessment model. *Environ Res*, 216, 114702. https://doi.org/10.1016/j.envres.2022.114702.

Im, U., Brandt, J., Geels, C., Hansen, K.M., Christensen, J.H., Andersen, M.S., Solazzo, E., Kioutsioukis, I., Alyuz, U., Balzarini, A., Baro, R., Bellasio, R., Bianconi, R., Bieser, J., Colette, A., Curci, G., Farrow, A., Flemming, J., Fraser, A., Jimenez-Guerrero, P., Kitwiroon, N., Liang, C.K., Nopmongcol, U., Pirovano, G., Pozzoli, L., Prank, M., Rose, R., Sokhi, R., Tuccella, P., Unal, A., Vivanco, M.G., West, J., Yarwood, G., Hogrefe, C., Galmarini, S. (2018). Assessment and economic valuation of air pollution impacts on human health over Europe and the United States as calculated by a multi-model ensemble in the framework of AQMEII3. *Atmos Chem Phys*, 18, 5967-5989. https://doi.org/10.5194/acp-18-5967-2018.

Im, U., Christensen, J.H., Nielsen, O.K., Sand, M., Makkonen, R., Geels, C., Anderson, C., Kukkonen, J., Lopez-Aparicio, S., Brandt, J. (2019). Contributions of Nordic anthropogenic emissions on air pollution and premature mortality over the Nordic region and the Arctic. *Atmos Chem Phys*, 19, 12975-12992. https://doi.org/10.5194/acp-19-12975-2019.

Jia, W., Zhang, X. (2021). Impact of modified turbulent diffusion of PM2.5 aerosol in WRF-Chem

simulations in eastern China. *Atmos Chem Phys*, 21, 16827-16841.
https://doi.org/10.5194/acp-21-16827-2021.

795 Joint, R.C., Institute, F.E.A.S., Orlandini, L., Kurokawa, J., Monni, S., Akimoto, H., Grano, D., Battye, B., Zuber, A., Pagliari, V., Janssens-Maenhout, G., Van Aardenne, J., Dentener, F., Keating, T., Klimont, Z., Wankmüller, R., Ohara, T. (2011). EDGAR-HTAP – A harmonized gridded air pollution emission dataset based on national inventories. https://pure.iiasa.ac.at/id/eprint/10114/.

800 Kaiser, J.W., Heil, A., Andreae, M.O., Benedetti, A., Chubarova, N., Jones, L., Morcrette, J.J., Razinger, M., Schultz, M.G., Suttie, M., van der Werf, G.R. (2012). Biomass burning emissions estimated with a global fire assimilation system based on observed fire radiative power. *Biogeosciences*, 9, 527-554. https://doi.org/10.5194/bg-9-527-2012.

Kumar, A., Patil, R.S., Dikshit, A.K., Kumar, R., Brandt, J., Hertel, O. (2016). Assessment of
805 impact of unaccounted emission on ambient concentration using DEHM and AERMOD in combination with WRF. *Atmos Environ (1994)*, 142, 406-413. https://doi.org/10.1016/j.atmosenv.2016.08.024.

Kumar, P., Beig, G., Singh, V., Sahu, S.K., Siingh, D., Bamniya, B.R. (2023). Model simulation of carbonaceous fine particulate matter using SAFAR emission inventory and comparison
810 with EDGAR-HTAP simulations. *Atmos Environ (1994)*, 315, 120147. https://doi.org/10.1016/j.atmosenv.2023.120147.

Lehtomäki, H., Geels, C., Brandt, J., Rao, S., Yaramenka, K., Åström, S., Andersen, M.S., Frohn, L.M., Im, U., Hänninen, O. (2020). Deaths Attributable to Air Pollution in Nordic Countries: Disparities in the Estimates. *Atmosphere (Basel)*, 11. https://doi.org/10.3390/atmos11050467.

815 Li, D., Wu, Y., Gross, B., Moshary, F. (2022). Dynamics of Mixing Layer Height and Homogeneity from Ceilometer-Measured Aerosol Profiles and Correlation to Ground Level PM2.5 in New York City. *Remote Sens (Basel)*, 14. https://doi.org/10.3390/rs14246370.

Li, S., Li, X., Deng, Z., Xia, X., Ren, G., An, D., Ayikan, M., Zhong, Y. (2023). Characteristics of atmospheric boundary layer and its relation with PM2.5 during winter in Shihezi, an Oasis
820 city in Northwest China. *Atmos Pollut Res*, 14, 101902. https://doi.org/10.1016/j.apr.2023.101902.

Lin, S., Tian, H., Hao, Y., Wu, B., Liu, S., Luo, L., Bai, X., Liu, W., Zhao, S., Hao, J., Guo, Z., Lv, Y. (2021). Atmospheric emission inventory of hazardous air pollutants from biomass direct-fired power plants in China: Historical trends, spatial variation characteristics, and
825 future perspectives. *Sci Total Environ*, 767, 144636. https://doi.org/10.1016/j.scitotenv.2020.144636.

Liu, F., Joo, T., Ditto, J.C., Saavedra, M.G., Takeuchi, M., Boris, A.J., Yang, Y., Weber, R.J., Dillner, A.M., Gentner, D.R., Ng, N.L. (2023). Oxidized and Unsaturated: Key Organic Aerosol Traits Associated with Cellular Reactive Oxygen Species Production in the
830 Southeastern United States. *Environ Sci Technol*, 57, 14150-14161. https://doi.org/10.1021/acs.est.3c03641.

Liu, J., Gao, X., Ruan, Z., Yuan, Y., Dong, S. (2022). Analysis of spatial and temporal distribution and influencing factors of fine particles in Heilongjiang Province. *Urban Clim*, 41, 101070. https://doi.org/10.1016/j.uclim.2021.101070.

835 Liu, J., Ruan, Z., Gao, X., Yuan, Y., Dong, S. (2022). Quantifying contribution of weather patterns to PM2.5 concentrations based on spatial effects and health risk assessment. *Sustain*

Cities Soc, 83, 103980. https://doi.org/10.1016/j.scs.2022.103980.

Liu, J., Ruan, Z., Gao, X., Yuan, Y., Dong, S., Li, X., Liu, X. (2023). Investigating the cumulative lag effects of environmental exposure under urban differences on COVID-19. *J Infect Public Health*. https://doi.org/10.1016/j.jiph.2023.06.002.

Liu, J., Ye, Z., Christensen, J.H., Dong, S., Geels, C., Brandt, J., Nenes, A., Yuan, Y., Im, U. (2024). Impact of anthropogenic emission control in reducing future PM2.5 concentrations and the related oxidative potential across different regions of China. *Sci Total Environ*, 918, 170638. https://doi.org/10.1016/j.scitotenv.2024.170638.

Liu, M., Saari, R.K., Zhou, G., Li, J., Han, L., Liu, X. (2021). Recent trends in premature mortality and health disparities attributable to ambient PM2.5 exposure in China: 2005–2017. *Environ Pollut*, 279, 116882. https://doi.org/10.1016/j.envpol.2021.116882.

Liu, Q., Baumgartner, J., Zhang, Y., Liu, Y., Sun, Y., Zhang, M. (2014). Oxidative Potential and Inflammatory Impacts of Source Apportioned Ambient Air Pollution in Beijing. *Environ Sci Technol*, 48, 12920-12929. https://doi.org/10.1021/es5029876.

Liu, Q., Lu, Z., Xiong, Y., Huang, F., Zhou, J., Schauer, J.J. (2020). Oxidative potential of ambient PM2.5 in Wuhan and its comparisons with eight areas of China. *Sci Total Environ*, 701, 134844. https://doi.org/10.1016/j.scitotenv.2019.134844.

Liu, S., Lim, Y., Pedersen, M., Jørgensen, J.T., Amini, H., Cole-Hunter, T., Mehta, A.J., So, R., Mortensen, L.H., Westendorp, R.G.J., Loft, S., Bräuner, E.V., Ketzel, M., Hertel, O., Brandt, J., Jensen, S.S., Christensen, J.H., Sigsgaard, T., Geels, C., Frohn, L.M., Brborić, M., Radonić, J., Sekulic, M.T., Bønnelykke, K., Backalarz, C., Simonsen, M.K., Andersen, Z.J. (2021). Long-term exposure to ambient air pollution and road traffic noise and asthma incidence in adults: The Danish Nurse cohort. *Environ Int*, 152, 106464. https://doi.org/10.1016/j.envint.2021.106464.

Liu, W., Xu, Y., Liu, W., Liu, Q., Yu, S., Liu, Y., Wang, X., Tao, S. (2018). Oxidative potential of ambient PM2.5 in the coastal cities of the Bohai Sea, northern China: Seasonal variation and source apportionment. *Environ Pollut*, 236, 514-528. https://doi.org/10.1016/j.envpol.2018.01.116.

Mao, J. (2017). Co-firing Biomass With Coal for Power Generation. *Distributed Energy*, 2. https://doi.org/10.16513/j.cnki.10-1427/tk.2017.05.008.

MEE. (2014). Ministry of Ecology and Environment. https://www.mee.gov.cn/. Accessed 11 January, 2023.

MEE. (2015). China Vehicle Emission Control Annual Report. https://www.mee.gov.cn/hjzl/sthjzk/ydyhjgl/201605/P020160513584304398771.pdf. Accessed 11 January, 2023.

MEE. (2020). Bulletin of the second National Survey of pollution sources. http://www.gov.cn/xinwen/2020-06/10/content_5518391.htm. Accessed 11 January, 2023.

Molina, C., Manzano, C.A., Toro A., R., Leiva G, M.A. (2023). The oxidative potential of airborne particulate matter in two urban areas of Chile: More than meets the eye. *Environ Int*, 173, 107866. https://doi.org/10.1016/j.envint.2023.107866.

Pietrogrande, M.C., Russo, M., Zagatti, E. (2019). Review of PM Oxidative Potential Measured with Acellular Assays in Urban and Rural Sites across Italy. *Atmosphere (Basel)*, 10, 626. https://doi.org/10.3390/atmos10100626.

Pui, D.Y.H., Chen, S., Zuo, Z. (2014). PM2.5 in China: Measurements, sources, visibility and

health effects, and mitigation. *Particuology*, 13, 1-26. https://doi.org/10.1016/j.partic.2013.11.001.

Puthussery, J.V., Singh, A., Rai, P., Bhattu, D., Kumar, V., Vats, P., Furger, M., Rastogi, N., Slowik, J.G., Ganguly, D., Prevot, A.S.H., Tripathi, S.N., Verma, V. (2020). Real-Time Measurements of PM2.5 Oxidative Potential Using a Dithiothreitol Assay in Delhi, India. *Environ Sci Technol Lett*, 7, 504-510. https://doi.org/10.1021/acs.estlett.0c00342.

Richter, J.H., Glanville, A.A., Edwards, J., Kauffman, B., Davis, N.A., Jaye, A., Kim, H., Pedatella, N.M., Sun, L., Berner, J., Kim, W.M., Yeager, S.G., Danabasoglu, G., Caron, J.M., Oleson, K.W. (2022). Subseasonal Earth System Prediction with CESM2. *Weather Forecast*, 37, 797-815. https://doi.org/10.1175/WAF-D-21-0163.1.

Shahpoury, P., Lelieveld, S., Johannessen, C., Berkemeier, T., Celo, V., Dabek-Zlotorzynska, E., Harner, T., Lammel, G., Nenes, A. (2024). Influence of aerosol acidity and organic ligands on transition metal solubility and oxidative potential of fine particulate matter in urban environments. *Sci Total Environ*, 906, 167405. https://doi.org/10.1016/j.scitotenv.2023.167405.

Shi, X., Zheng, Y., Lei, Y., Xue, W., Yan, G., Liu, X., Cai, B., Tong, D., Wang, J. (2021). Air quality benefits of achieving carbon neutrality in China. *Sci Total Environ*, 795, 148784. https://doi.org/10.1016/j.scitotenv.2021.148784.

Skamarock, W.C., Klemp, J.B., Dudhia, J., Gill, D.O., Barker, D.M., Duda, M.G., Huang, X., Wang, W., Powers, J.G. (2008). A description of the advanced research WRF version 3. *NCAR technical note*, 475, 113. http://dx.doi.org/10.5065/D68S4MVH.

Skamarock, W.C., Klemp, J.B., Dudhia, J., Gill, D.O., Liu, Z., Berner, J., Huang, X.Y. (2021). A Description of the Advanced Research WRF Model Version 4.3 (No. NCAR/TN-556+STR). http://dx.doi.org/10.5065/1dfh-6p97.

Soares, J., Sofiev, M., Geels, C., Christensen, J.H., Andersson, C., Tsyro, S., Langner, J. (2016). Impact of climate change on the production and transport of sea salt aerosol on European seas. *Atmos Chem Phys*, 16, 13081-13104. https://doi.org/10.5194/acp-16-13081-2016.

Song, M., Oh, S., Park, C., Bae, M. (2021). analytical procedure for dithiothreitol-based oxidative potential of PM2. 5. *Asian J Atmos Environ*, 15, 2021015. https://doi.org/10.5572/ajae.2021.015.

Strand, A., Hov, Ø. (1994). A two-dimensional global study of tropospheric ozone production. *Journal of Geophysical Research: Atmospheres*, 99, 22877-22895. https://doi.org/10.1029/94JD01945.

Tang, L., Xue, X., Qu, J., Mi, Z., Bo, X., Chang, X., Wang, S., Li, S., Cui, W., Dong, G. (2020). Air pollution emissions from Chinese power plants based on the continuous emission monitoring systems network. *Sci Data*, 7, 325. https://doi.org/10.1038/s41597-020-00665-1.

Thomas, D.C., Christensen, J.H., Massling, A., Pernov, J.B., Skov, H. (2022). The effect of the 2020 COVID-19 lockdown on atmospheric black carbon levels in northeastern Greenland. *Atmos Environ (1994)*, 269, 118853. https://doi.org/10.1016/j.atmosenv.2021.118853.

Thomas, S.R., Nicolau, S., Martínez-Alvarado, O., Drew, D.J., Bloomfield, H.C. (2021). How well do atmospheric reanalyses reproduce observed winds in coastal regions of Mexico? *Meteorol Appl*, 28, e2023. https://doi.org/10.1002/met.2023.

Tong, D., Zhang, Q., Liu, F., Geng, G., Zheng, Y., Xue, T., Hong, C., Wu, R., Qin, Y., Zhao, H., Yan, L., He, K. (2018). Current Emissions and Future Mitigation Pathways of Coal-Fired

925   Power Plants in China from 2010 to 2030. *Environ Sci Technol*, 52, 12905-12914. https://doi.org/10.1021/acs.est.8b02919.

    Upadhyay, A., Dey, S., Goyal, P. (2020). A comparative assessment of regional representativeness of EDGAR and ECLIPSE emission inventories for air quality studies in India. *Atmos Environ (1994)*, 223, 117182. https://doi.org/10.1016/j.atmosenv.2019.117182.

930   van Donkelaar, A., Hammer, M.S., Bindle, L., Brauer, M., Brook, J.R., Garay, M.J., Hsu, N.C., Kalashnikova, O.V., Kahn, R.A., Lee, C., Levy, R.C., Lyapustin, A., Sayer, A.M., Martin, R.V. (2021). Monthly Global Estimates of Fine Particulate Matter and Their Uncertainty. *Environ Sci Technol*, 55, 15287-15300. https://doi.org/10.1021/acs.est.1c05309.

    Wang, G., Deng, J., Zhang, Y., Zhang, Q., Duan, L., Hao, J., Jiang, J. (2020). Air pollutant
935   emissions from coal-fired power plants in China over the past two decades. *Sci Total Environ*, 741, 140326. https://doi.org/10.1016/j.scitotenv.2020.140326.

    Wang, J., Lin, X., Lu, L., Wu, Y., Zhang, H., Lv, Q., Liu, W., Zhang, Y., Zhuang, S. (2019). Temporal variation of oxidative potential of water soluble components of ambient PM2.5 measured by dithiothreitol (DTT) assay. *Sci Total Environ*, 649, 969-978.
940   https://doi.org/10.1016/j.scitotenv.2018.08.375.

    Wen, W., Hua, T., Liu, L., Liu, X., Ma, X., Shen, S., Deng, Z. (2023). Oxidative Potential Characterization of Different PM2.5 Sources and Components in Beijing and the Surrounding Region. *Int J Environ Res Public Health*, 20, 5109. https://doi.org/10.3390/ijerph20065109.

    Xing, C., Wang, Y., Yang, X., Zeng, Y., Zhai, J., Cai, B., Zhang, A., Fu, T., Zhu, L., Li, Y.,
945   Wang, X., Zhang, Y. (2023). Seasonal variation of driving factors of ambient PM2.5 oxidative potential in Shenzhen, China. *Sci Total Environ*, 862, 160771. https://doi.org/10.1016/j.scitotenv.2022.160771.

    Xu, J., Martin, R.V., Evans, G.J., Umbrio, D., Traub, A., Meng, J., van Donkelaar, A., You, H., Kulka, R., Burnett, R.T., Godri Pollitt, K.J., Weichenthal, S. (2021). Predicting Spatial
950   Variations in Multiple Measures of Oxidative Burden for Outdoor Fine Particulate Air Pollution across Canada. *Environ Sci Technol*, 55, 9750-9760. https://doi.org/10.1021/acs.est.1c01210.

    Xu, X., Frey, S.K., Ma, D. (2022). Hydrological performance of ERA5 and MERRA-2 precipitation products over the Great Lakes Basin. *Journal of Hydrology: Regional Studies*,
955   39, 100982. https://doi.org/10.1016/j.ejrh.2021.100982.

    Yang, F., Liu, C., Qian, H. (2021). Comparison of indoor and outdoor oxidative potential of PM2.5: pollution levels, temporal patterns, and key constituents. *Environ Int*, 155, 106684. https://doi.org/10.1016/j.envint.2021.106684.

    Yu, H., Puthussery, J.V., Wang, Y., Verma, V. (2021). Spatiotemporal variability in the oxidative
960   potential of ambient fine particulate matter in the Midwestern United States. *Atmos Chem Phys*, 21, 16363-16386. https://doi.org/10.5194/acp-21-16363-2021.

    Yu, S., Liu, W., Xu, Y., Yi, K., Zhou, M., Tao, S., Liu, W. (2019). Characteristics and oxidative potential of atmospheric PM2.5 in Beijing: Source apportionment and seasonal variation. *Sci Total Environ*, 650, 277-287. https://doi.org/10.1016/j.scitotenv.2018.09.021.

965   Yun, X., Shen, G.F., Shen, H.Z., Meng, W.J., Chen, Y.L., Xu, H.R., Ren, Y., Zhong, Q.R., Du, W., Ma, J.M., Cheng, H.F., Wang, X.L., Liu, J.F., Wang, X.J., Li, B.G., Hu, J.Y., Wan, Y., Tao, S. (2020). Residential solid fuel emissions contribute significantly to air pollution and associated health impacts in China. *Sci Adv*, 6. https://www-science-

org.ez.statsbiblioteket.dk/doi/10.1126/sciadv.aba7621.

970 Zare, A., Christensen, J.H., Gross, A., Irannejad, P., Glasius, M., Brandt, J. (2014). Quantifying the contributions of natural emissions to ozone and total fine PM concentrations in the Northern Hemisphere. *Atmos Chem Phys*, 14, 2735-2756. https://doi.org/10.5194/acp-14-2735-2014.

Zare, A., Christensen, J.H., Irannejad, P., Brandt, J. (2012). Evaluation of two isoprene emission
975 models for use in a long-range air pollution model. *Atmos Chem Phys*, 12, 7399-7412. https://doi.org/10.5194/acp-12-7399-2012.

Zeng, Z., Gui, K., Wang, Z., Luo, M., Geng, H., Ge, E., An, J., Song, X., Ning, G., Zhai, S., Liu, H. (2021). Estimating hourly surface PM2.5 concentrations across China from high-density meteorological observations by machine learning. *Atmos Res*, 254, 105516.
980 https://doi.org/10.1016/j.atmosres.2021.105516.

Zhang, H., Li, N., Tang, K., Liao, H., Shi, C., Huang, C., Wang, H., Guo, S., Hu, M., Ge, X. (2022). Estimation of secondary PM 2.5 in China and the United States using a multi-tracer approach. *Atmos Chem Phys*, 22, 5495-5514. https://doi.org/10.5194/acp-2021-683.

Zhang, L., Hu, X., Chen, S., Chen, Y., Lian, H. (2023). Characterization and source apportionment
985 of oxidative potential of ambient PM2.5 in Nanjing, a megacity of Eastern China. *Env Pollut Bioavail*, 35, 2175728. https://doi.org/10.1080/26395940.2023.2175728.

Zheng, B., Tong, D., Li, M., Liu, F., Hong, C.P., Geng, G.N., Li, H.Y., Li, X., Peng, L.Q., Qi, J., Yan, L., Zhang, Y.X., Zhao, H.Y., Zheng, Y.X., He, K.B., Zhang, Q. (2018). Trends in China's anthropogenic emissions since 2010 as the consequence of clean air actions. *Atmos*
990 *Chem Phys*, 18, 14095-14111. https://doi.org/10.5194/acp-18-14095-2018.

Zheng, Y., Alapaty, K., Herwehe, J.A., Del Genio, A.D., Niyogi, D. (2016). Improving High-Resolution Weather Forecasts Using the Weather Research and Forecasting (WRF) Model with an Updated Kain–Fritsch Scheme. *Mon Weather Rev*, 144, 833-860. https://doi.org/10.1175/MWR-D-15-0005.1.

995 Zhu, Y., Huang, L., Li, J., Ying, Q., Zhang, H., Liu, X., Liao, H., Li, N., Liu, Z., Mao, Y., Fang, H., Hu, J. (2018). Sources of particulate matter in China: Insights from source apportionment studies published in 1987–2017. *Environ Int*, 115, 343-357. https://doi.org/10.1016/j.envint.2018.03.037.